mTOR complex 1 controls the nuclear localization and function of glycogen synthase kinase 3β

Received for publication, March 9, 2018, and in revised form, July 19, 2018 Published, Papers in Press, July 30, 2018, DOI 10.1074/jbc.RA118.002800

Stephen J. Bautista[‡], Ivan Boras[‡], Adriano Vissa[§¶], Noa Mecica[‡], Christopher M. Yip[§‖], Peter K. Kim[¶‖], and Costin N. Antonescu[‡ ‡‡1]**

*From the [‡]Department of Chemistry and Biology and Graduate Program in Molecular Science, Ryerson University, Toronto, Ontario M5B 2K3, the [‡‡]Keenan Research Centre for Biomedical Science of St. Michael's Hospital, Toronto, Ontario M5B 1W8, the [§]Institute of Biomaterials and Biomedical Engineering, University of Toronto, Toronto, Ontario M5S 3E5, the [¶]Program in Cell Biology, Hospital for Sick Children, Toronto, Ontario M5G 0A4, the [‖]Department of Biochemistry, University of Toronto, Toronto, Ontario M5G 1X8, and the **Department of Chemical Engineering and Applied Chemistry, University of Toronto, Toronto, Ontario M5S 3E5, Canada*

Edited by Phyllis I. Hanson

Glycogen synthase kinase 3β (GSK3β) phosphorylates and thereby regulates a wide range of protein substrates involved in diverse cellular functions. Some GSK3β substrates, such as c-Myc and Snail, are nuclear transcription factors, suggesting the possibility that GSK3β function is controlled through its nuclear localization. Here, using ARPE-19 and MDA-MB-231 human cell lines, we found that inhibition of mTOR complex 1 (mTORC1) leads to partial redistribution of GSK3β from the cytosol to the nucleus and to a GSK3β-dependent reduction of the levels of both c-Myc and Snail. mTORC1 is known to be controlled by metabolic cues, such as by AMP-activated protein kinase (AMPK) or amino acid abundance, and we observed here that AMPK activation or amino acid deprivation promotes GSK3β nuclear localization in an mTORC1-dependent manner. GSK3β was detected on several distinct endomembrane compartments, including lysosomes. Consistently, disruption of late endosomes/lysosomes through a perturbation of RAS oncogene family member 7 (Rab7) resulted in loss of GSK3β from lysosomes and in enhanced GSK3β nuclear localization as well as GSK3β-dependent reduction of c-Myc levels. These findings indicate that the nuclear localization and function of GSK3β is suppressed by mTORC1 and suggest a link between metabolic conditions sensed by mTORC1 and GSK3β-dependent regulation of transcriptional networks controlling cellular biomass production.

Glycogen synthase kinase 3β (GSK3β)[2] is a serine/threonine protein kinase that controls numerous aspects of cellular physiology such as proliferation, metabolism, and apoptosis (1–4). Dysregulation of GSK3β has been linked to various diseases such as insulin resistance/diabetes, Alzheimer's disease, and cancer (5). GSK3β phosphorylates over 100 substrates, more than the typical number of substrates for most kinases (1, 4, 6), thus illustrating the broad capabilities for control of cell physiology by GSK3β. Notably, GSK3β is further distinguished from other kinases by being basally active (2). Hence, many mechanisms probably exist to regulate GSK3β.

GSK3β activity is indeed regulated by phosphorylation on Ser-9, mediated by kinases such as Akt, protein kinase C, and p90RSK, resulting in negative regulation of GSK3β activity (7–12). Phosphorylation of other sites on GSK3β may also suppress GSK3β activity, such as that of Ser-389 by p38 MAPK (13). In addition to GSK3β phosphorylation, control of GSK3β action may be achieved by localization of GSK3β or some of its substrates into distinct cellular compartments, such as the nucleus, such that GSK3β may have limited and regulated access to certain substrates (4, 14, 15).

Several GSK3β substrates are transcription factors (4) localized largely to the nucleus, including c-Myc (16), Snail (17), C/EBPα and -β (18, 19), and CREB (20). c-Myc controls genes important for proliferation, metabolism, and biomass production and stem-cell self-renewal (for reviews, see Refs. 21–23). Moreover, c-Myc is an oncogene altered in many cancers (23), highlighting the need for precise regulation of its function. c-Myc protein levels are controlled by GSK3β-dependent phosphorylation of Thr-58 on c-Myc (16), leading to ubiquitin-dependent proteosomal degradation (24). Control of phosphorylation and/or degradation of these nuclear substrates by GSK3β may involve modulation of GSK3β nuclear localization. However, the identity of the cellular compartments in which GSK3β is localized and how it moves from various cellular compartments to the nucleus is not well-defined.

GSK3β localizes in part to membrane compartments in the cytoplasm. It is recruited to the plasma membrane via association with Axin (25), impacting Wnt signaling to β-catenin (26). GSK3β is also detected on APPL1 early endosomes (27). APPL1

This work was supported by a Discovery Grant from the Natural Sciences and Engineering Research Council of Canada; an Early Researcher Award from the Ontario Ministry of Research, Innovation, and Science; and a New Investigator Award from the Canadian Institutes of Health Research (to C. N. A.). The authors declare that they have no conflicts of interest with the contents of this article.

This article contains Figs. S1–S4.

[1] To whom correspondence should be addressed: Ryerson University, 350 Victoria St., Toronto, Ontario M5B 2K3, Canada. Tel.: 416-979-5000 (ext. 4659); E-mail: cantonescu@ryerson.ca.

[2] The abbreviations used are: GSK3, glycogen synthase kinase; PI3K, phosphatidylinositol 3-kinase; NLS, nuclear localization sequence; mTOR, mechanistic target of rapamycin; mTORC1, mTOR complex 1; TSC, tuberous sclerosis complex; AMPK, AMP-activated protein kinase; EBSS, Earle's balanced salt solution; SIM, structured illumination microscopy; DAPI, 4′,6-diamidino-2-phenylindole; HA, hemagglutinin.

acts as an adaptor protein to recruit Akt, facilitating GSK3β phosphorylation and inactivation on these early endosomes, thus impacting clathrin-mediated endocytosis (28) and cell survival (27). GSK3β also localizes to lysosomes (29) and controls lysosomal acidification (30). Hence, GSK3β may localize to multiple distinct endomembrane compartments including the plasma membrane, early endosomes, and lysosomes, with distinct functions at each locale.

GSK3β exhibits nuclear localization under certain conditions including in response to apoptotic signals induced by heat shock or staurosporine treatment (31), S-phase of the cell cycle (32), replicative senescence in fibroblasts (33), and loss of phosphatidylinositol 3-kinase (PI3K)-Akt signaling in embryonic stem cells (15). Site-directed mutagenesis studies revealed that nuclear localization of GSK3β requires a bipartite nuclear localization sequence (NLS) contained within residues 85–103 on GSK3β and that nuclear localization was also modulated by the N-terminal 9 amino acids on GSK3β (14).

Collectively, these observations raise the question of whether the control of GSK3β nucleocytoplasmic shuttling could be an important mechanism to control its function by modulating access to nuclear substrates. Indeed, nuclear localization of GSK3β induced by inhibition of PI3K or Akt leads to GSK3β-dependent phosphorylation of c-Myc, leading to its degradation (15). However, it is not clear how PI3K–Akt signals impact GSK3β localization. Because this N-terminal region contains the Ser-9 phosphorylation site, it is possible that Akt or other kinases capable of phosphorylation of this residue impact nuclear localization of GSK3β, although a GSK3β mutant (S9A) did not show obvious differences in nuclear localization (14).

Whereas Akt may control GSK3β localization via direct phosphorylation of GSK3β on Ser-9, this may be indirect and result from Akt-dependent activation of other signals, downstream of Akt, such as the mTOR complex 1 (mTORC1). Mitogenic activation of PI3K–Akt signals leads to inhibition of the tuberous sclerosis complex 1/2 (TSC 1/2) (34), activation of the GTPase Rheb (35), and thus mTORC1 activation (36, 37). mTORC1 in turn controls many processes, including metabolism, protein synthesis, cell growth, and autophagy (recently reviewed by Saxton and Sabatini (38)). In addition to mitogenic control, mTORC1 is also strongly controlled by metabolic cues. Amino acid levels are sensed by a mechanism involving the lysosomal V-ATPase and other sensors, leading to the recruitment and activation of mTORC1 at the lysosome under conditions of amino acid sufficiency (39, 40). Further, activation of AMP-activated protein kinase (AMPK) by energy insufficiency, resulting from an increase in the cellular levels of AMP and ADP relative to ATP, leads to phosphorylation and activation of TSC2, thus suppressing mTORC1 (41, 42). Hence, mitogenic and metabolic signals control mTORC1 activation.

Although it is not known whether PI3K–Akt signaling regulates GSK3β nuclear localization via engagement of mTORC1, several studies have reported that GSK3β enhances mTORC1 activity. GSK3β phosphorylates the mTORC1 subunit Raptor (43), resulting in enhanced mTORC1 activity (30, 43). GSK3β also negatively regulates mTORC1 signaling by binding (44) and phosphorylation of TSC2 (42). Moreover, GSK3β binds to and regulates AMPK (45). Hence, GSK3β controls the mTORC1 and AMPK metabolic and mitogenic sensors. However, the possibility of a reciprocal regulation of GSK3β by signals from mTORC1 and AMPK, impacting GSK3β nuclear localization and thus access to substrates therein, such as c-Myc, has so far been unexamined.

Here, we examine mTORC1 regulation of GSK3β nuclear localization and function. To do so, we use pharmacological and other approaches to manipulate mitogenic or metabolic signals and examine GSK3β localization to various endomembrane compartments and nucleus as well as GSK3β-dependent functions associated with nuclear GSK3β. We find a novel regulatory axis sensing mitogenic signals, metabolic cues, and membrane traffic at the late endosome/lysosome that modulates GSK3β nuclear localization and function.

Results

The PI3K–Akt signaling pathway controls GSK3β nucleocytoplasmic shuttling and thus access of GSK3β to nuclear targets either directly or via activation of the downstream kinase mTORC1. mTORC1 integrates both mitogenic (PI3K–Akt) and metabolic cues and is localized to the lysosome once activated. Using a variety of strategies to manipulate mitogenic and metabolic signals converging on mTORC1 and lysosomal membrane traffic, we examined how mTORC1 regulates GSK3β nuclear access and function.

mTORC1 controls GSK3β nuclear localization and c-Myc levels

To determine whether mTORC1 regulates GSK3β localization and function downstream of PI3K/Akt, we first examined the effect of the mTORC1 inhibitor rapamycin on c-Myc levels. Treatment of ARPE-19 cells (henceforth referred to as RPE cells) with 1 μg/ml rapamycin caused a time-dependent decrease in c-Myc levels, reaching 57 ± 4.8% after 2 h of rapamycin treatment ($n = 6$, $p < 0.05$; Fig. 1*A*). Importantly, co-treatment with a 10 μM concentration of the GSK3β kinase inhibitor CHIR99021 blunted the decrease in c-Myc levels elicited by rapamycin treatment (Fig. 1*A*). Consistent with this result, rapamycin treatment also elicited a reduction in levels of the transcription factor Snail, an effect also blunted by co-treatment with CHIR99021 (Fig. 1*B*).

We next used siRNA gene silencing of GSK3β, which resulted in a 91 ± 4.7% reduction of GSK3β protein levels ($n = 3$, $p < 0.05$; Fig. S1*A*). Whereas RPE cells also express the paralog GSK3α, silencing of GSK3β was specific and did not impact expression of GSK3α (Fig. S1*B*). Cells subjected to silencing of GSK3β exhibited no change in c-Myc upon inhibition of sequential signals in the PI3K–Akt–mTORC1 axis, achieved by treatment with either LY294002, Akti-1/2, or rapamycin, respectively (Fig. 1*C*). In contrast, each inhibitor effectively reduced c-Myc levels in cells subjected to nontargeting (control) siRNA treatment (Fig. 1*C*). Taken together, these results indicate that PI3K–Akt signals converge on mTORC1 to enhance c-Myc levels in a manner that requires the regulation of GSK3β.

To determine how PI3K–Akt–mTORC1 signals control c-Myc levels in a GSK3β-dependent manner, we examined the localization and levels of endogenous GSK3β and c-Myc. Con-

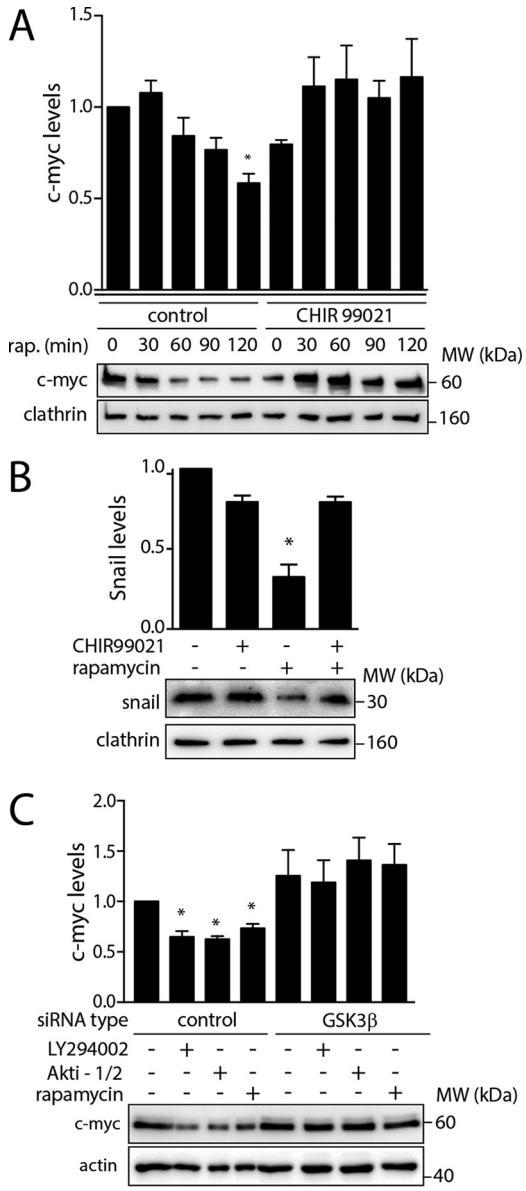

Figure 1. mTORC1 inhibition decreases c-Myc and Snail levels in a GSK3β-dependent manner. *A* and *B*, RPE cells were treated with 1 μM rapamycin, in the presence or absence of 10 μM CHIR 99021 for the indicated times (*A*) or 1 h (*B*). Shown are representative immunoblots of whole-cell lysates probed with anti-c-Myc (*A*), anti-Snail (*B*), or anti-clathrin heavy chain (load) antibodies. Also shown are mean c-Myc levels ± S.E. (*error bars*) ($n = 6$; *, $p < 0.05$) (*A*) or mean Snail levels ($n = 3$; *, $p < 0.05$) (*B*) relative to that in the control conditions (absence of CHIR99021 and rapamycin). *C*, RPE cells were transfected with siRNA targeting GSK3β or nontargeting siRNA (control) and then treated with either 10 μM LY294002, 5 μM Akti-1/2, or 1 μM rapamycin for 1 h. Shown are representative immunoblots of whole-cell lysates probed with anti-c-Myc or anti-actin (load) antibodies as well as mean c-Myc levels ($n = 4$). *, $p < 0.05$ relative to that in the control conditions (absence of LY294002, Akti1/2, and/or rapamycin). All Western blotting quantifications shown have been normalized to loading controls (clathrin or actin).

sistent with previous reports (14, 15, 31–33), in cells grown in serum (*e.g.* with an active PI3K–Akt–mTORC1 axis), GSK3β primarily localizes within the cytosol and appears mostly excluded from the nucleus (Fig. 2*A*). We confirmed the specificity of detection of endogenous GSK3β by immunofluorescence microscopy following GSK3β silencing (Fig. S1*C*). In contrast, and as expected (46–48), c-Myc localizes virtually entirely within the nucleus under these conditions (Fig. 2*A*). Thus, under conditions in which mTORC1 is active, GSK3β and c-Myc are compartmentalized separately within the cytosol and nucleus, respectively.

We next determined how PI3K–Akt–mTORC1 signaling regulates GSK3β localization. Treatment of RPE cells with either LY294002, Akti-1/2, or rapamycin to perturb PI3K, Akt, or mTORC1, respectively, resulted in a robust and significant ($n = 3$, $p < 0.05$) increase in nuclear GSK3β, measured by the ratio of nuclear to cytosolic mean fluorescence intensities of GSK3β, which we term the GSK3β nuclear localization index (Fig. 2*B*). Importantly, the effect of rapamycin treatment on GSK3β nuclear translocation and Snail protein levels was also observed in MDA-MB-231 breast cancer cells (Fig. S1, *D* and *E*), demonstrating that the mTORC1-dependent control of GSK3β is not unique to RPE cells. Similar observations were made when detecting GSK3β cytoplasmic and nuclear localization by subcellular fractionation (Fig. 2*C*). Furthermore, inhibition of the PI3K–Akt–mTORC1 axis also resulted in robust nuclear localization of GSK3α (Fig. 2*D*), a paralog of GSK3β with highly similar kinase domains but unique terminal motifs (3, 49). These results indicate that PI3K–Akt signals act via control of mTORC1 to regulate GSK3β nuclear localization as well as that of GSK3α.

To test the importance of Ran in mTORC1-dependent GSK3β nuclear translocation, we examined the impact of Ran GTP-binding mutants on GSK3β localization. We expressed WT Ran or one of two Ran mutants, Ran T24N and G19V, which are constitutively GDP- or GTP-bound, respectively (50). Cells expressing WT Ran exhibited little nuclear GSK3β in the control condition, but a robust localization of GSK3β in the nucleus was observed upon treatment with rapamycin (Fig. 3, *top panels*; quantification shown in the *bottom panel*). In contrast, cells expressing Ran T24N exhibited nuclear GSK3β in both control and rapamycin-treated conditions (Fig. 3), consistent with Ran-GDP acting to facilitate nuclear import (50). Further, cells expressing Ran G19V exhibited mostly cytosolic GSK3β in both control and rapamycin-treated conditions, consistent with this mutant blocking Ran-dependent nuclear import (Fig. 3). These experiments confirm that the change in localization of GSK3β observed upon treatment with rapamycin indeed corresponds to nuclear translocation. Further, these results indicate that GSK3β undergoes Ran-dependent nucleocytoplasmic shuttling and Ran-dependent nuclear import that is regulated by mTORC1.

Metabolic cues regulate GSK3β nuclear localization via mTORC1

As mTORC1 is regulated by both mitogenic (PI3K–Akt) signals as well as metabolic cues, we next examined how each of these signals contributes to the control of GSK3β nuclear localization. AMPK is activated via ATP insufficiency and negatively regulates mTORC1 signaling through phosphorylation and activation of TSC2 (41, 42). Consistent with the effects of mTORC1 inhibition by rapamycin, treatment with the AMPK activator A769662 resulted in robust GSK3β nuclear localization (Fig. 4*A*). Importantly, AMPK and mTORC1 exhibit reciprocal negative regulation (51). As such, GSK3β nuclear localization could conceivably be the direct result of loss of

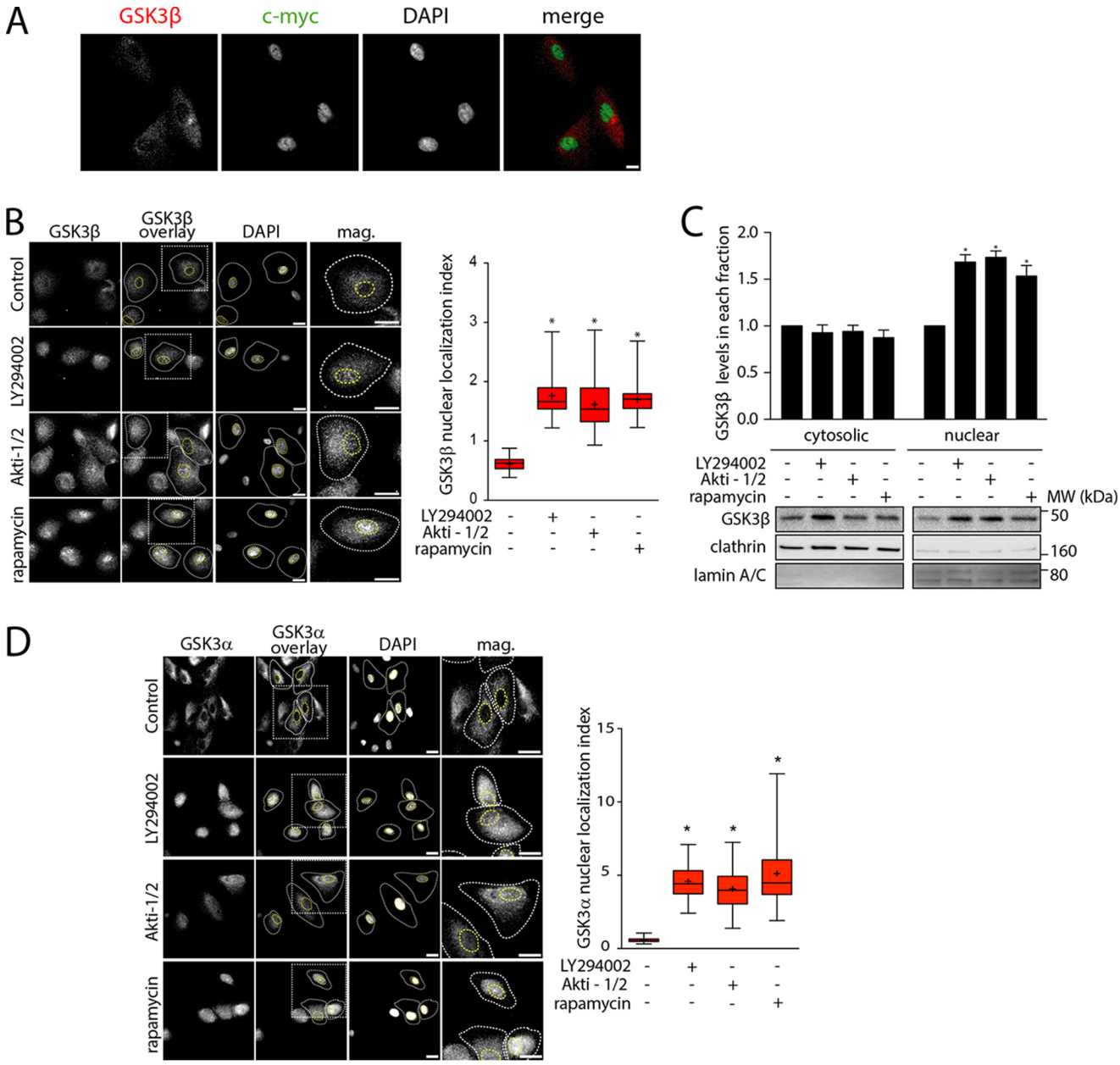

Figure 2. Inhibition of PI3K/Akt/mTORC1 signals promotes GSK3β nuclear localization. *A*, representative images obtained by wide-field epifluorescence microscopy of control RPE cells (no inhibitor treatment) stained to detect endogenous GSK3β or c-Myc, with DAPI stain to identify the nucleus. *Scale bar*, 20 μm. *B–D*, RPE cells were treated with either 10 μM LY294002, 5 μM Akti-1/2, or 1 μM rapamycin for 1 h. Following this treatment, cells were then fixed and stained to detect endogenous GSK3β (*B*) or GSK3α (*D*). Shown for each (*left panels*) are micrographs obtained by wide-field epifluorescence microscopy representative of three independent experiments. *Scale bar*, 20 μm. Also shown for each condition as *GSK3β* (or α) *overlay* are sample cellular and nuclear outlines, and a *box* corresponding to a magnified image of a single cell. Also shown (*right panel*) is the mean GSK3β or GSK3α nuclear localization index ± S.E. (*error bars*) ($n = 3$, >30 cells/condition/experiment); *, $p < 0.05$ relative to control conditions (absence of LY294002, Akti1/2, and rapamycin). Shown in *C* are Western blots of cytosolic and nuclear fractions and mean nuclear GSK3β values ± S.E. ($n = 3$). *, $p < 0.05$.

mTORC1 signals or an increase in AMPK activation, both of which would be expected to occur upon treatment with either rapamycin or A769662. To dissect a role for mTORC1 *versus* AMPK in control of GSK3β nuclear localization, we used the AMPK inhibitor compound C (52). Cells treated with compound C exhibited a rapamycin-dependent increase in GSK3β nuclear localization comparable with that observed in cells treated with rapamycin but not compound C (Fig. 4*A*). This indicates that AMPK activity is dispensable for GSK3β nuclear localization induced by mTORC1 inhibition. As GSK3β forms a complex with AMPK (45), we also tested whether AMPK may have a kinase-independent, structural role in regulation of GSK3β. However, silencing of AMPK did not impact GSK3β nuclear localization (Fig. S2). Collectively, these results indicate that whereas AMPK activation also triggers an accumulation of nuclear GSK3β, this occurs as a result of AMPK-dependent inhibition of mTORC1 signals, and not as a result of direct action of AMPK on GSK3β nuclear localization.

mTORC1 is activated by abundance of amino acids in a manner that requires the V-ATPase (39). To determine how amino acid-dependent activation of mTORC1 impacted control of GSK3β localization, we treated cells with the V-ATPase inhib-

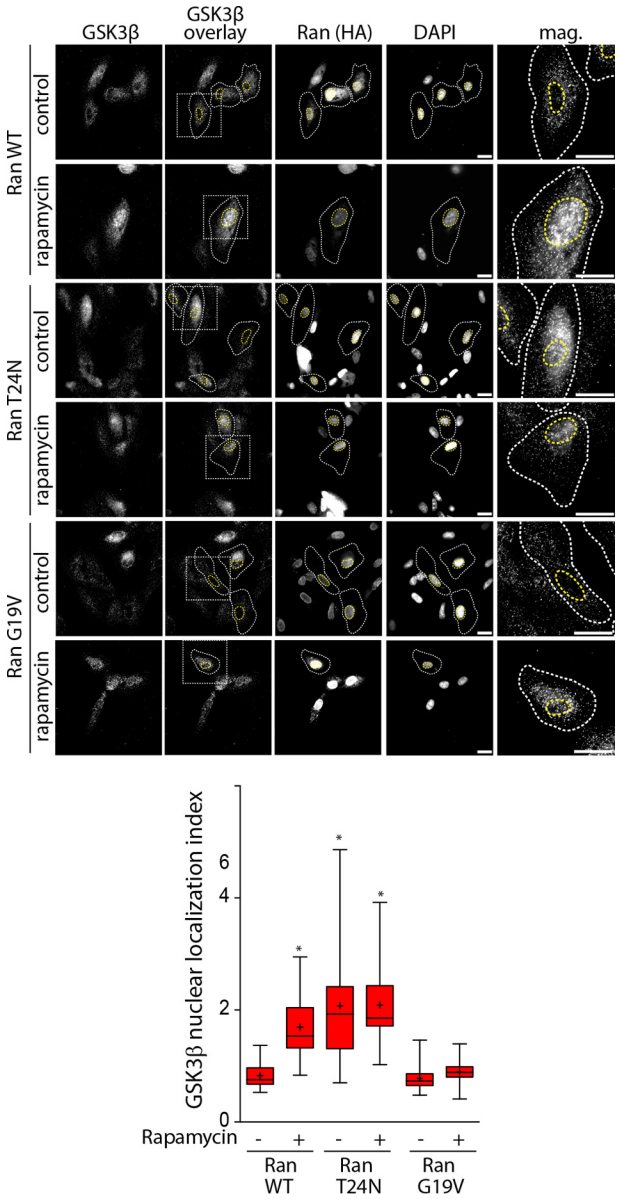

Figure 3. Rapamycin-induced GSK3β nuclear localization is Ran-dependent. RPE cells were transfected with plasmids encoding HA-tagged WT, T24N, or G19V Ran and then treated with 1 μM rapamycin for 1 h, followed by detection of endogenous GSK3β and exogenous HA-tagged Ran proteins. Shown (*top*) are micrographs obtained by wide-field epifluorescence microscopy representative of three independent experiments. *Scale bar*, 20 μm. Also shown for each condition as *GSK3β overlay* are sample cellular and nuclear outlines and a *box* corresponding to a magnified image of a single cell. Also shown (*bottom*) is the mean GSK3β nuclear localization index ± S.E. (*error bars*) ($n = 3$, >30 cells/condition/experiment); *, $p < 0.05$ relative to control conditions (no rapamycin treatment).

itor concanamycin A. Cells treated with concanamycin A exhibited a significant enhancement of nuclear GSK3β relative to control (Fig. 4*B*). Consistent with this result, amino acid deprivation achieved via incubation of cells in amino acid–depleted medium (Earle's balanced salt solution (EBSS)) also mimicked the effect of rapamycin treatment in RPE (Fig. 4*C*) as well as MDA-MB-231 (Fig. S1*C*) cells. These results indicate that amino acid sensing by mTORC1 contributes to the regulation of GSK3β nuclear localization.

mTORC1 inhibition also leads to induction of autophagy (53). We therefore tested whether autophagy is required for GSK3β nuclear localization upon mTORC1 inhibition with rapamycin. To inhibit autophagy induction, we treated cells with siRNA targeting endogenous ULK (54), which resulted in a robust 77 ± 6.2% reduction of ULK expression ($n = 3$, $p < 0.05$; Fig. S3*A*). Cells treated with siRNA to silence ULK1 exhibited cytosolic GSK3β, which relocalized to the nucleus upon rapamycin treatment in a manner indistinguishable from cells treated with nontargeting siRNA (Fig. 4*D*). As autophagy induction has also been reported to lead to c-Myc degradation (55), we also tested the effect of ULK1 silencing on rapamycin-induced c-Myc levels. Surprisingly, silencing of ULK1 on its own reduced c-Myc levels (Fig. S3*B*). Moreover, and in contrast to the findings of a previous study (55), impairment of autophagy induction by ULK1 silencing did not prevent the rapamycin-induced reduction in c-Myc levels (Fig. S3*B*). Thus, GSK3β nuclear translocation and c-Myc degradation observed upon mTORC1 inhibition are largely independent of autophagy induction. Instead, c-Myc degradation upon mTORC1 inhibition is mediated by regulation of GSK3β nuclear localization and function.

Control of GSK3β nuclear localization does not require GSK3β Ser-9 phosphorylation

Akt phosphorylates GSK3β on Ser-9, which negatively regulates GSK3β kinase activity toward certain substrates. We next examined how GSK3β phosphorylation may contribute to control of GSK3β nuclear localization by mTORC1. As expected, cells treated with LY294002 or Akti-1/2 exhibited significant reduction in GSK3β Ser-9 phosphorylation by 80 ± 0.8 and 60 ± 6.8%, respectively ($n = 3$, $p < 0.05$; Fig. 5*A*). In contrast, cells treated with rapamycin exhibited no change in GSK3β Ser-9 phosphorylation compared with control (Fig. 5*A*). These results uncouple Ser-9 phosphorylation from control of GSK3β nuclear localization. To directly probe the contribution of GSK3β Ser-9 phosphorylation to mTORC1-dependent GSK3β nuclear localization, we studied the subcellular localization of GSK3β S9A. Under basal conditions, GSK3β S9A remains cytosolic, whereas treatment with the Akt inhibitor Akti-1/2 resulted in nuclear localization of GSK3β S9A, as seen with GSK3β WT (Fig. 5*B*).

Using phos-tag acrylamide electrophoresis, a technique that exaggerates differences in apparent molecular weight of phosphorylated species of a protein (56), we observed two detectable species of GSK3β, of which the higher molecular weight species probably corresponds to the Ser-9–phosphorylated form given its sensitivity to PI3K and Akt inhibition (Fig. S4*A*). In contrast and as expected, rapamycin had no effect on GSK3β detected by this method. Collectively, these results indicate that regulation of GSK3β Ser-9 phosphorylation does not contribute to control of GSK3β nuclear localization by PI3K–Akt–mTORC1 signals.

GSK3β is localized to several distinct membrane compartments within the cytoplasm

Active mTORC1 is recruited to the surface of the lysosome (57). Together with our observations that mTORC1 controls GSK3β nuclear localization, this suggests that (i) mTORC1 control of GSK3β may occur at lysosomes and (ii) control of

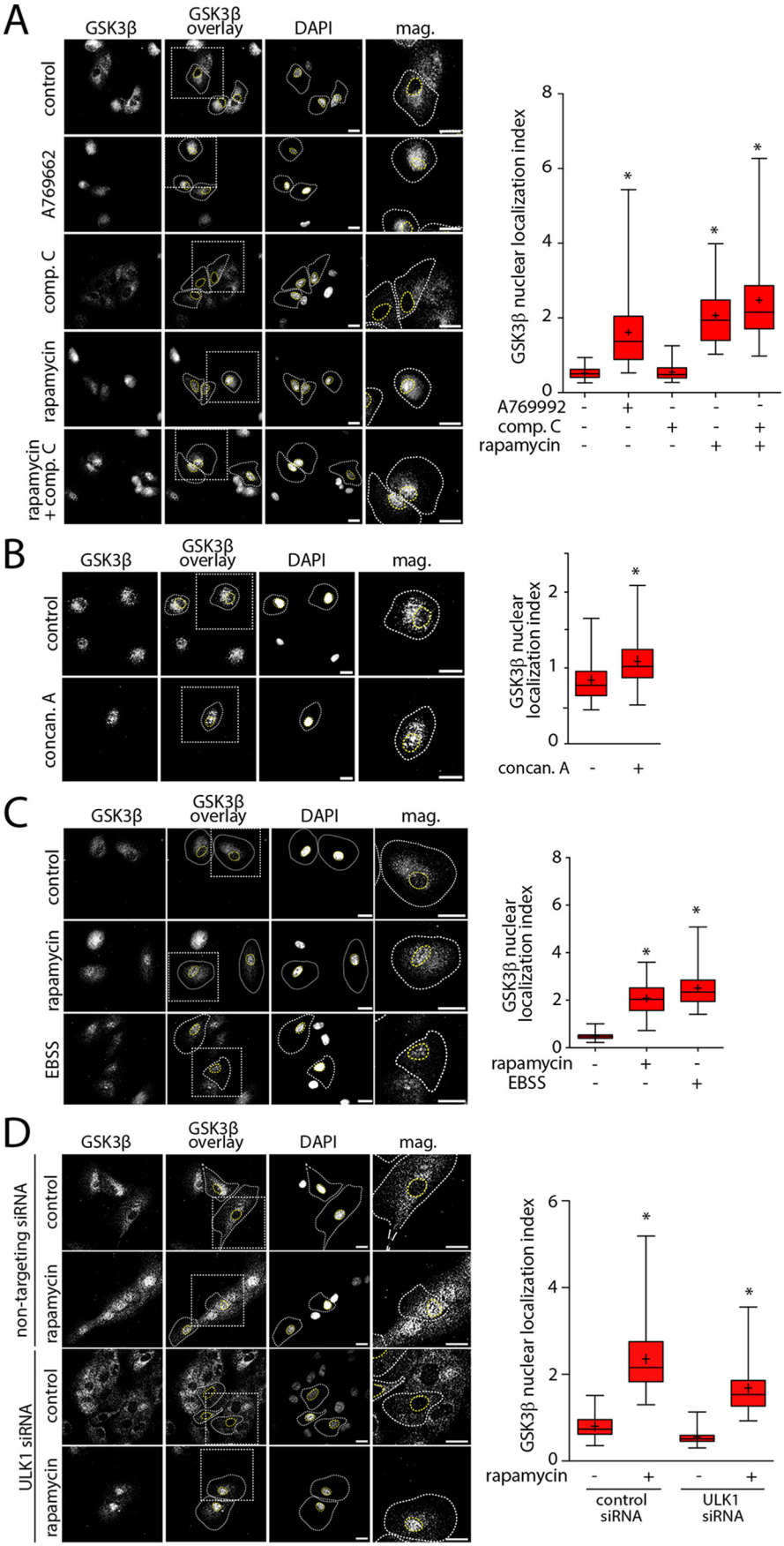
A
GSK3β
GSK3β overlay
DAPI
mag.
control
A769662
comp. C
rapamycin
rapamycin + comp. C
GSK3β nuclear localization index
A769992
comp. C
rapamycin
B
concan. A
C
EBSS
D
non-targeting siRNA
ULK1 siRNA
control siRNA
ULK1 siRNA

GSK3β nuclear localization by mTORC1 may require lysosomal membrane traffic. To determine whether a pool of GSK3β is indeed localized to lysosomes concomitantly to GSK3β recruitment to other endomembrane compartments, we systematically examined the localization of endogenous GSK3β relative to APPL1 and EEA1 early endosomes and to lysosomes demarked by LAMP1. We observed punctate distribution of endogenous GSK3β within the cytoplasm, with some visible overlap with each of APPL1, EEA1, and LAMP1 (Fig. 6, *A–C*, *left panels*). To determine whether the overlap observed between GSK3β and each marker was specific, we used quantification by Manders' coefficient to compare overlap between real pairs of image channels, as well as between pairs of images with scrambled channel spatial position. This revealed specific GSK3β recruitment to each membrane compartment (Fig. 6, *A–C*). We performed a similar colocalization analysis of the image data using Pearson's coefficient and obtained similar results (Fig. S4*B*). This indicates that GSK3β indeed exhibits partial yet specific localization to several distinct endomembrane compartments, including APPL1 and EEA1 early endosomes and late endosomes/lysosomes demarked by LAMP1.

To further examine how GSK3β may localize to lysosomes, we employed structured illumination microscopy (SIM). Using this method, we were able to resolve the limiting membrane of lysosomes demarked by LAMP1 fluorescence staining (Fig. 6*D*). Importantly, GSK3β fluorescence staining was readily observed in punctate structures, some of which were associated with lysosomes. Using automated segmentation of the lysosomes in SIM images, GSK3β puncta were preferentially detected on the limiting membrane *versus* the interior of lysosomes (Fig. 6*D*). These results indicate that a subset of GSK3β in the cytoplasm exhibits association with the lysosome, either restricted to subdomains of the lysosomal surface (58) or in structures associated with the lysosome, such as within membrane contact sites (59).

Control of GSK3β nuclear localization and c-Myc levels requires normal lysosomal membrane traffic

Given the localization of mTORC1 (57) and partial localization of GSK3β (Fig. 6, *C* and *D*) to or near the lysosome, we next sought to determine the role of late endosome/lysosome membrane traffic in mTORC1-dependent control of GSK3β nuclear localization. To do so, we used a Rab7 mutant that is constitutively GDP-bound (T22N), which disrupts membrane traffic at the late endosome/lysosome (60). Cells expressing Rab7 T22N exhibited a significant increase in nuclear GSK3β, even in the absence of rapamycin treatment, compared with cells expressing Rab7 WT (Fig. 7*A*). Furthermore, cells expressing Rab7 T22N exhibited a depletion of GSK3β from lysosomes, observed by overlap of endogenous GSK3β and LAMP1, quantified by Manders' coefficient (Fig. S4*D*). In contrast to the nuclear accumulation of GSK3β in cells expressing Rab7 T22N, silencing of APPL1 (Fig. S4*C*) to disrupt early endosome membrane traffic did not impact GSK3β nuclear localization (Fig. 7*B*). These results indicate that membrane traffic at the late endosome/lysosome may be important to organize mTORC1 signals leading to control of GSK3β nuclear localization.

To determine the consequence of Rab7-dependent control of GSK3β nuclear localization, we examined the effect of expression of Rab7 T22N on GSK3β-dependent c-Myc levels. Cells expressing Rab7 T22N exhibited a stark reduction in c-Myc levels relative to cells expressing Rab7 WT (Fig. 7*C*). Importantly, treatment of cells expressing Rab7 T22N with the GSK3β inhibitor CHIR99021 restored c-Myc levels to that observed in cells expressing Rab7 WT (Fig. 7*C*). Taken together, these results indicate that control of GSK3β nuclear localization requires Rab7-dependent late endosome/lysosomal membrane traffic, reflecting perhaps the role of lysosomes as platforms for mTORC1 signaling required to negatively regulate GSK3β nuclear translocation.

Discussion

We identified that the nuclear localization of GSK3β is regulated by mTORC1, such that conditions that reduce mTORC1 activity result in increased nuclear localization of GSK3β and increased GSK3β-dependent degradation of nuclear substrates, such as c-Myc and Snail (Fig. 8). Furthermore, GSK3β was partly but specifically localized to the surface of late endosomes/lysosomes, and perturbation of membrane traffic at the late endosomes/lysosomes disrupted GSK3β nucleocytoplasmic shuttling and regulation of c-Myc levels.

Localization of GSK3β to multiple membrane compartments within the cytoplasm

Separate studies have reported that GSK3β may localize to a number of distinct cellular compartments, including endomembranes, mitochondria, and the nucleus (reviewed by Beurel *et al.* (1)). By a systematic, unbiased approach, we find that endogenous GSK3β localizes to several distinct endomembrane compartments, including APPL1 endosomes, EEA1-positive early endosomes, and LAMP1-positive late endosomes/lysosomes (Fig. 6). In each case, the overlap of GSK3β immunofluorescence signal and that of each compartment marker is clearly limited and partial, with substantial proportions of each signal not exhibiting overlap (Fig. 6, *A–C*). However, systematic and unbiased analysis of colocalization performed by Manders' (Fig. 6, *A–C*) or Pearson's (Fig. S4*B*) coefficient analysis indicates that GSK3β overlap with each compartment is specific and nonrandom. Moreover, the specific recruitment of GSK3β to the limiting membrane of

Figure 4. mTORC1 integrates multiple signals to control GSK3β nuclear localization. RPE cells were treated with either 100 μM A769662, 5 μM compound C, or 1 μM rapamycin, alone or in combination for 1 h (*A*); with 1 μM concanamycin for 1 h (*B*); or with amino acid-free EBSS medium for 2 h (*C*). *D*, RPE cells were transfected with siRNA targeting ULK1 or nontargeting siRNA (control). Following knockdown, RPE cells were treated with 1 μM rapamycin for 1 h and then were fixed and stained to detect endogenous GSK3β. Shown for each of these (*left*) are micrographs obtained by wide-field epifluorescence microscopy representative of three independent experiments. *Scale bar*, 20 μm. Also shown for each condition as *GSK3β overlay* are sample cellular and nuclear outlines and a *box* corresponding to a magnified image of a single cell. Also shown (*right*) is the mean GSK3β nuclear localization index ± S.E. (*error bars*) ($n = 3$ independent experiments, >30 cells/condition/experiment). *, $p < 0.05$ relative to the noninhibitor-treated condition (and in the control siRNA sample for *D*) of each experiment.

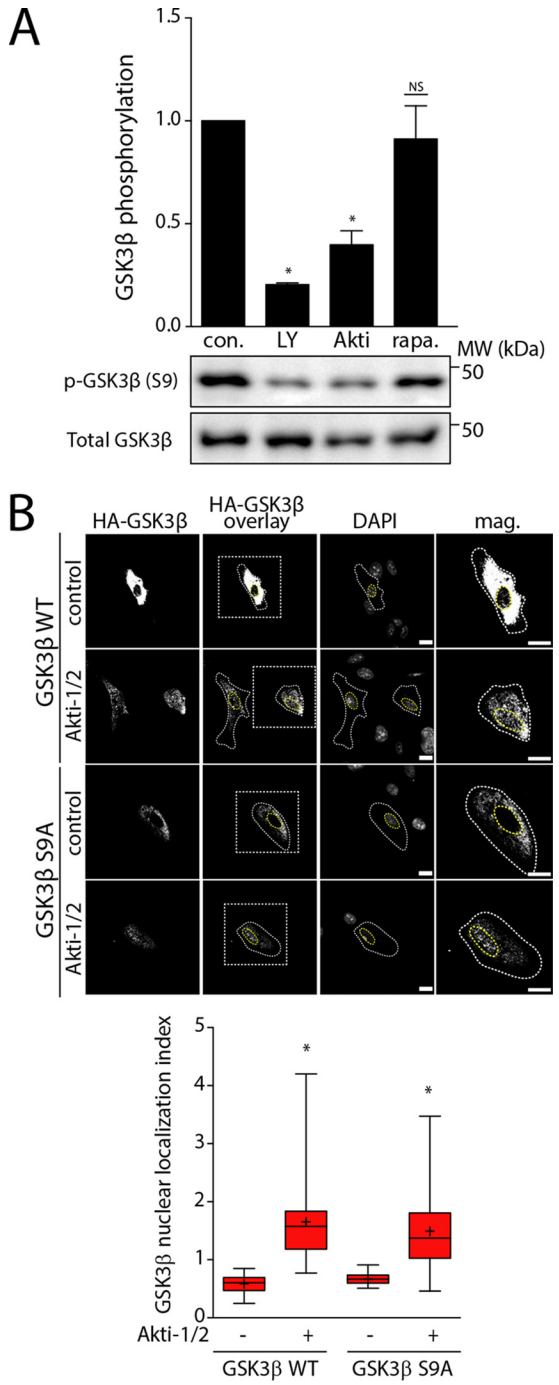

Figure 5. GSK3β Ser-9 phosphorylation is not required for GSK3β nuclear localization induced by inhibition of PI3K–Akt–mTORC1 signals. *A*, RPE cells were treated with either 10 μM LY294002, 5 μM Akti-1/2, or 1 μM rapamycin for 1 h. Shown are representative immunoblots of whole-cell lysates probed with anti-pSer-9 GSK3β or anti-total GSK3β antibodies. Also shown are mean anti-pSer-9 GSK3β levels (normalized to total GSK3β) ± S.E. (*error bars*) ($n = 3$); *, $p < 0.05$ relative to that in the control conditions (absence of LY294002, Akti1/2, and rapamycin). *B*, RPE cells were transfected with plasmids encoding HA-tagged WT or S9A GSK3β and then treated with 5 μM Akti-1/2 for 1 h, followed by detection of exogenous HA-GSK3β proteins. Shown (*top*) are micrographs obtained by wide-field epifluorescence microscopy representative of three independent experiments. *Scale bar*, 20 μm. Also shown for each condition as *HA-GSK3β overlay* are sample cellular and nuclear outlines and a *box* corresponding to a magnified image of a single cell. Also shown (*bottom*) is the mean HA-GSK3β nuclear localization index ± S.E. ($n = 3$, >30 cells/condition/experiment); *, $p < 0.05$ relative to control conditions (absence of Akti1/2 treatment). All Western blotting quantifications shown have been normalized to loading controls.

LAMP1-positive late endosomes/lysosomes is supported by images obtained by SIM and unbiased analysis of the localization of GSK3β within the lysosome (Fig. 6*D*), as well as by the observation that perturbation of late endosome/lysosome membrane traffic by expression of a dominant interfering mutant of Rab7 abolishes the overlap of GSK3β with LAMP1 signals (Fig. S4*D*). Our observations are thus consistent with the notion that GSK3β is localized to a number of distinct cellular compartments, with a minor pool that in some cases is <10% of total cellular GSK3β, recruited to each such compartment at steady state.

Our observations are also consistent with previous studies showing GSK3β localization to APPL1 endosomes (27). APPL1 recruitment to a subset of internalized membranes formed by clathrin-mediated endocytosis precedes the acquisition of markers of the EEA1 early endosome (61). This pool of GSK3β within APPL1 endosomes may be specifically targeted by phosphorylation on Ser-9 by Akt, as silencing of APPL1 abolishes Akt-dependent GSK3β phosphorylation (27, 28). Notably, perturbation of APPL1 by silencing did not impact mTORC1-dependent control of GSK3β nuclear localization (Fig. 7*B*), suggesting that the APPL1-localized pool of GSK3β does not directly participate in the regulation of GSK3β nuclear localization by mTORC1.

As mTORC1 localizes to the surface of late endosomes and lysosomes, the pool of GSK3β on these membranes may be under direct regulation by mTORC1 to control GSK3β nucleocytoplasmic shuttling. Indeed, a previous report had observed some overlap of GSK3β and the lysosome (29). However, GSK3β may also be sequestered within intraluminal vesicles of multivesicular bodies in response to Wnt signaling (62), raising the possibility that the overlap that we observed by spinning disc confocal microscopy between LAMP1-positive structures and GSK3β (Fig. 6*C*) could reflect GSK3β within intraluminal vesicles. However, quantification of SIM images suggests that GSK3β at lysosomes is preferentially associated with the limiting membrane of these organelles, and not the lumen (Fig. 6*D*). Moreover, perturbation of Rab7 disrupts the localization of GSK3β and LAMP1 (Fig. S4*C*), yet Rab7 disruption does not impact the sequestration of material into intraluminal vesicles (63). The molecular mechanism(s) by which GSK3β is recruited to the surface of lysosomes remains unknown and is beyond the scope of this study. Our results thus add systematic analysis and quantification to indicate that a pool of GSK3β is present on the limiting membrane of the lysosome, suggesting that this pool may be subject to regulation by mTORC1, resulting in control of GSK3β nuclear localization.

Mechanism of control of GSK3β nuclear localization by mTORC1

We found that direct inhibition of any component of the PI3K–Akt–mTORC1 axis or activation of AMPK to trigger mTORC1 inhibition results in an increase in GSK3β nuclear localization. Moreover, perturbation of Rab7-dependent membrane traffic also resulted in an increase in GSK3β nuclear localization, suggesting that in addition to mTORC1 signals, lysosomal traffic and/or organization is also required to control

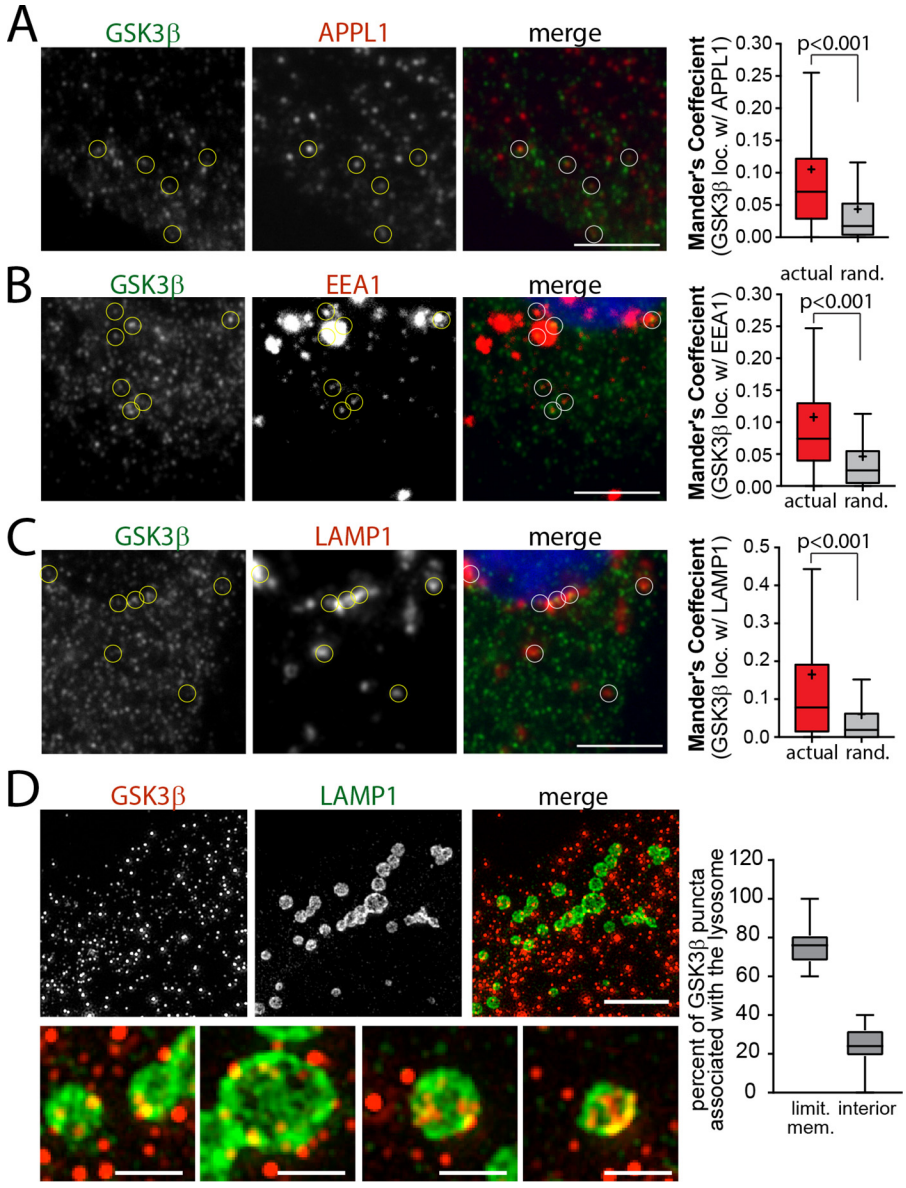

Figure 6. GSK3β exhibits partial localization to several distinct endomembrane compartments. *A–C*, RPE cells were fixed and stained to detect endogenous GSK3β, together with either endogenous APPL1 (*A*), EEA1 (*B*), or LAMP1 (*C*). Shown are representative images obtained by spinning-disc confocal microscopy, corresponding to a *z*-section through the middle of the cell. *Scale bar*, 20 μm (*left panels*). Also shown (*right panels*) are the median (*bar*), interquartile range (*boxes*) and full range (*bars*) of Manders' coefficients to measure overlap of GSK3β signals with either APPL1 (*A*), EEA1 (*B*), or LAMP1 (*C*) (n = 3, > 30 cells/condition/experiment). For each image set, Manders' coefficients were calculated for actual images (*actual*), as well as images in which the spatial position of one of the channels had been randomized (*rand.*), to allow resolution of specific GSK3β localization to various endomembrane compartments from random overlap of signals in a field densely populated with fluorescent objects. *D*, RPE cell samples prepared similarly as in *C* were subjected to SIM. Shown (*left*) are representative micrographs of (endogenous) GSK3β and LAMP1 staining morphology. *Scale bar*, 5 μm (*top panels*) or 1 μm (*bottom panel*). Also shown (*right panels*) is the distribution of GSK3β puncta following automated segmentation of the lysosome in SIM images into limiting membrane and interior, shown are the median (*bar*), interquartile range (*boxes*), and full range (*bars*) of GSK3β puncta in each region for each lysosome.

GSK3β nuclear import. Interestingly, we also observed that inhibition of PI3K–Akt–mTORC1 also increased nuclear localization of GSK3α. Hence, it is likely that mTORC1 signals similarly gate GSK3α and GSK3β nuclear localization. GSK3α nuclear localization was proposed to be uniquely regulated by a calcium- and calpain-dependent mechanism, dependent on its N terminus (64). However, both GSK3α (64) and GSK3β (15) were reported to undergo nuclear translocation in response to serum withdrawal, consistent with our observations of a central role for mTORC1 in control of GSK3α/β nuclear localization, which we report here. Taken together, we propose that mTORC1 establishes a form of "molecular licensing" for retention within the cytoplasm for GSK3α and GSK3β, resulting in nuclear exclusion under conditions of elevated mTORC1 activity. This molecular licensing could take the form of a post-translational modification of GSK3α or GSK3β or of regulation of protein complex formation at specific subcellular locale(s).

GSK3β undergoes nucleocytoplasmic shuttling, due to nuclear import in balance with FRAT-1–mediated nuclear export (65). Nuclear import of some (but not all) proteins is controlled by a gradient of GTP-bound and GDP-bound

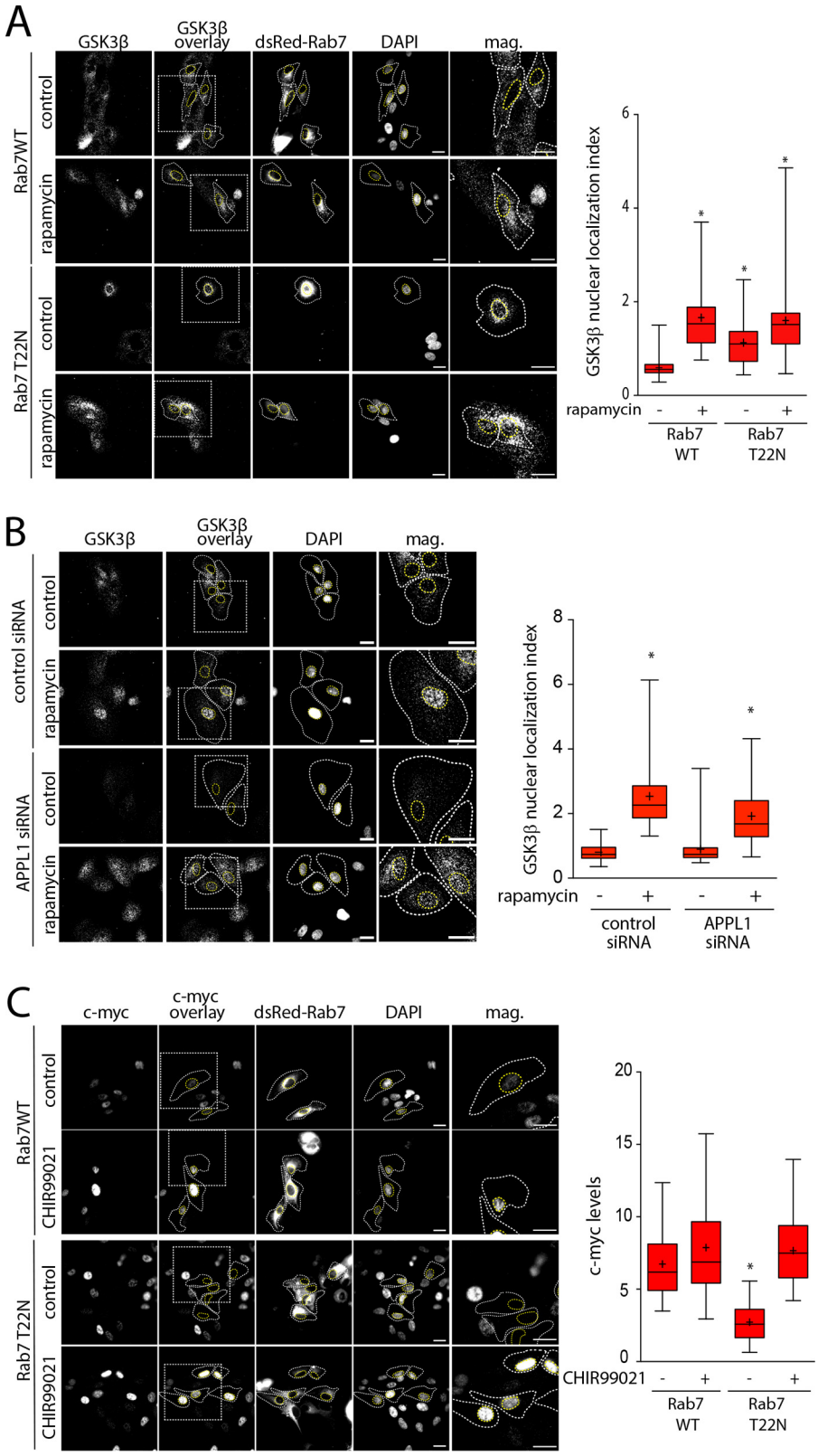

Figure 7. Rab7 controls GSK3β nuclear localization and GSK3β-dependent c-Myc levels. RPE cells were transfected with plasmids encoding dsRed-tagged WT or T22N Rab7 (*A* and *C*) or transfected with siRNA targeting APPL1 or nontargeting siRNA (control) (*B*). Some samples were then treated with 1 μM rapamycin for 1 h, followed by detection of endogenous GSK3β (*A* and *B*) or c-Myc (*C*). Shown (*left panels*) are micrographs obtained by wide-field epifluorescence microscopy representative of three independent experiments. *Scale bar*, 20 μm. Also shown for each condition as GSK3β overlay (*A*) or c-Myc overlay (*B*) are sample cellular and nuclear outlines and a *box* corresponding to a magnified image of a single cell. Also shown (*right panels*) is the mean ± S.E. (*error bars*) of the GSK3β nuclear localization index (*A* and *B*) ($n = 3$, >30 cells/condition/experiment) or total cellular c-Myc level (*C*) ($n = 3$, >30 cells/condition/experiment); *, $p < 0.05$ relative to control conditions (no rapamycin or CHIR99021 treatment).

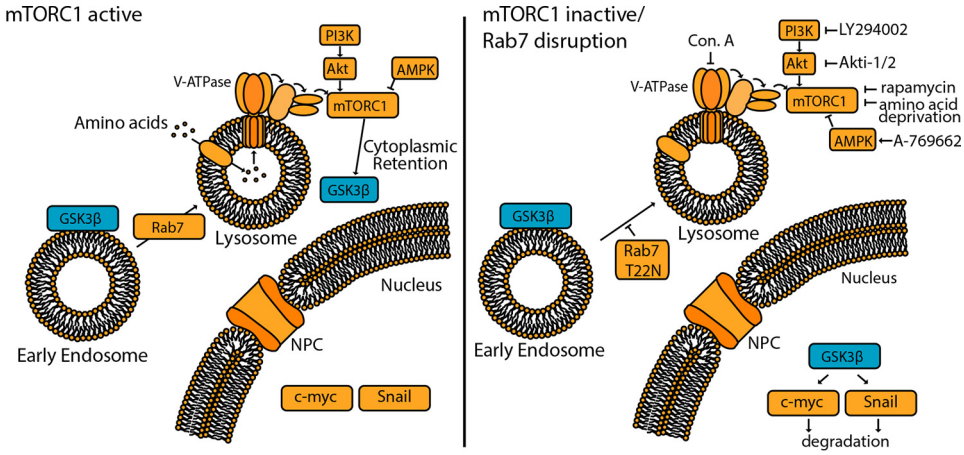

Figure 8. Model depicting signals and processes regulating GSK3β nucleocytoplasmic shuttling. Shown on the *left* is an mTORC1-active state, in which GSK3β is largely excluded from the nucleus. Shown on the *right* is an mTORC1-inactive or Rab7-perturbed state, in which GSK3β accumulates in the nucleus and is thus able to phosphorylate direct substrates, such as c-Myc and Snail. Also shown are the known targets of various inhibitors or other pharmacological agents used in this study that impact mTORC1 signaling. See "Results" and "Discussion" for more details. *NPC*, nuclear pore complex

Ran that spans the nuclear membrane (66). By expression of mutants of Ran (Fig. 3), we show that the nucleocytoplasmic shuttling of GSK3β is Ran-dependent. Nuclear import of GSK3β resulting from mTORC1 inhibition by rapamycin was prevented in cells expressing Ran G19V mutant defective in GTP hydrolysis and thus defective in nuclear import. Hence, nuclear import of GSK3β regulated by mTORC1 is Ran-dependent.

We examined whether the phosphorylation of Ser-9 on GSK3β could control its mTORC1-regulated nuclear localization; however, two observations strongly suggest that this is not the case: (i) inhibition of mTORC1 by rapamycin did not alter Ser-9 phosphorylation of GSK3β (Fig. 5*A*), and (ii) a mutant of GSK3β that cannot be phosphorylated at this position (S9A) behaved similarly to WT with respect to mTORC1-dependent nuclear localization (Fig. 5*B*), similar to a previous report with this GSK3β mutant (14). GSK3β can also be phosphorylated on a number of other residues, including Tyr-216, which may result from autophosphorylation at the time of GSK3β synthesis (1). Further, GSK3β can be phosphorylated at Thr-43 (67) and Ser-389 (13) by Erk and p38 MAPK, respectively, each of which lead to reduction in GSK3β activity. Notably, using a phos-tag gel electrophoresis approach, a technique that exacerbates the apparent molecular weight increase caused by phosphorylation, we were only able to resolve two bands for GSK3β that probably correspond to Ser-9 –phosphorylated and non-Ser-9 –phosphorylated forms (Fig. S4*A*). It will be interesting to determine in future studies whether and how phosphorylation at sites other than Ser-9 is regulated by mTORC1 to control GSK3β nuclear localization.

Other than phosphorylation, other modifications reported for GSK3β include citrullination (68), ADP-ribosylation (69), and calpain cleavage (70). Indeed, citrullination of Arg-3 and Arg-5 residues within GSK3β is important for nuclear localization (68). However, we observed that mTORC1 controls both GSK3α and GSK3β nuclear localization, and these two GSK3 paralogs differ at their N terminus within the region of GSK3β that undergoes citrullination. Hence, it appears unlikely that mTORC1 controls citrullination of GSK3β as a mechanism of control of its nucleocytoplasmic shuttling. Although beyond the scope of this study, it will be interesting to note how future work may resolve whether mTORC1-dependent regulation of post-translational modification of GSK3β underlies the regulation of its nuclear localization by mTORC1.

mTORC1-dependent control of GSK3β nuclear localization may occur as a result of regulation of GSK3β interaction with other proteins in various endomembrane compartments. It is worth noting that the vast majority of cytoplasmic, but not nuclear, GSK3β is associated with another protein(s) (14). Thus, it is possible that control of GSK3β nucleocytoplasmic shuttling involves regulation of protein–protein interactions that serve to occlude the bipartite NLS of GSK3β (residues 85–103) (14), thus limiting GSK3β nuclear localization when these interactions are present.

We also found that Rab7 is required to retain GSK3β in the cytoplasm under conditions when mTORC1 is otherwise active. Importantly, disruption of late endosome/lysosome membrane traffic by perturbations of Rab7 or other proteins does not impact mTORC1 activity (71). This indicates that the ability of mTORC1 to limit the nuclear localization of GSK3β requires active traffic to the late endosome/lysosome. This in turn suggests that the protein interactions engaged by GSK3β that occlude its NLS and thus limit nuclear localization may occur on the lysosome, consistent with our observed localization of GSK3β to the lysosome. Indeed, GSK3α and GSK3β have nearly identical kinase domains (in which the NLS is found), consistent with the ability of mTORC1 to gate nuclear access for both GSK3 paralogs.

Furthermore, our observations that mTORC1 controls GSK3β nuclear localization add to previous reports that GSK3β activates mTORC1 signals (42) and suggest the existence of reciprocal regulation of mTORC1 and GSK3β. Overall, we propose that mTORC1 signals limit the ability of GSK3β to localize to the nucleus and that this may result from mTORC1-dependent control of GSK3β interactions with other proteins in a manner that regulates occlusion of the NLS of GSK3β at the lysosome.

Regulation of GSK3β nuclear functions by mTORC1

We identified that various metabolic and mitogenic signals gate nuclear access for GSK3β. This in turn allows for GSK3β-dependent regulation of nuclear substrates in response to mTORC1 signals. Previous studies reported that nuclear and cytoplasmic pools of GSK3β have distinct functions, such as nuclear GSK3β facilitating stem cell differentiation over self-renewal (15) or the cytosolic pool of GSK3β being sufficient to mediate GSK3β-dependent cell survival to tumor necrosis factor α apoptotic signals (14).

One of the nuclear substrates of GSK3β is c-Myc, a helix-loop-helix leucine zipper transcription factor that has a very short half-life (15–30 min) (23, 72). As previously reported, nuclear localization of GSK3β is required for phosphorylation of c-Myc on Thr-58, resulting in enhanced c-Myc degradation (16). We show that rapamycin treatment, which promotes nuclear localization of GSK3β, also results in an acute reduction in c-Myc accumulation (Fig. 1), most likely due to c-Myc degradation. A previous report suggested that rapamycin treatment elicits degradation of c-Myc by induction of autophagy, as a result of regulation of AMBRA-dependent dephosphorylation of c-Myc at Ser-62 (55). However, we show that the degradation of c-Myc induced by rapamycin is insensitive to impairment of autophagy induction elicited by siRNA gene silencing of ULK1 (Fig. 4*D*). Moreover, we find that the rapamycin-induced reduction in c-Myc levels is countered by either chemical inhibition or silencing of GSK3β (Fig. 1, *A* and *B*). Hence, our results indicate that mTORC1-dependent control of GSK3β nuclear localization regulates c-Myc in a manner that does not require induction of autophagy.

Based on the control of GSK3β nuclear localization by mTORC1 leading to control of c-Myc, we propose the existence of a metabolic sensing signaling network that links nutrient availability with biomass production and proliferation. Indeed, c-Myc controls the expression of many genes, generally to promote ribosome production, biomass accumulation, and enhanced cellular bioenergetics, such as through mitochondrial biosynthesis (73). Furthermore, c-Myc promotes epithelial–mesenchymal transition (74). Hence, signals activated during nutrient deficiency can impair the anabolic c-Myc–dependent promotion of biomass accumulation via this novel mTORC1–GSK3β–c-Myc signaling axis involving control of GSK3β nuclear localization.

GSK3β may also regulate other nuclear substrates selectively during conditions of reduced mTORC1 signaling or other states in which GSK3β exhibits nuclear localization. Collectively, regulation of other GSK3β substrates, such as Snail (leading to degradation (75)) or c-Jun (leading to impaired DNA binding (76)), is consistent with the effect of GSK3β-dependent degradation of c-Myc: reduced cell cycle progression, impairment of epithelial–mesenchymal transition, and/or reduced biomass accumulation. Whereas examination of mTORC1-dependent regulation of all known GSK3β nuclear targets is beyond the scope of this study, it is perhaps tempting to speculate that metabolic and mitogenic signals broadly control the nuclear profile of GSK3β functions, coordinating energy-demanding accumulation of biomass, cell cycle progression, and growth with nutrient availability. As cancer cells exhibit heterogeneity of metabolic cues and signals, it is possible that differences in metabolism between cancer cells that result in distinct GSK3β nuclear localization profiles may underlie in part the differences in response to drugs targeting GSK3β in cancer, although this remains to be examined.

In conclusion, we identified that GSK3β nucleocytoplasmic shuttling is controlled by both mitogenic signals, such as PI3K–Akt and metabolic cues including amino acid or ATP availability as a result of mTORC1-dependent control of GSK3β nuclear import. In addition, GSK3β localized in part to the late endosome/lysosome, and nuclear localization of GSK3β was regulated by Rab7, suggesting that membrane traffic at late endosomes and lysosomes impacts signals leading to control of GSK3β nuclear localization. Last, we propose that GSK3β-dependent control of nuclear proteins by mTORC1 occurs by regulation of GSK3β nuclear import, linking nutrient availability to control of energy-dependent transcriptional networks.

Experimental procedures

Materials

Antibodies targeting specific proteins were obtained as follows: GSK3β (catalog no. 9832), GSK3α (catalog no. 4815), GSK3α/β (catalog no. 5676) phospho-GSK3β (Ser-9; catalog no. 9323), actin (catalog no. 8456), HA epitope (catalog no. 3724 or 2367), EEA1 (catalog no. 3288), LAMP1 (catalog no. 15665), APPL1 (catalog no. 3858), ULK1 (catalog no. 8054) (Cell Signaling, Danvers, MA), and clathrin (sc-12734) and lamin A/C (sc-6215) (Santa Cruz Biotechnology, Inc., Dallas, TX). Horseradish peroxidase or fluorescently conjugated secondary antibodies were purchased from Cell Signaling Technology (Danvers, MA). DAPI nuclear staining was purchased from Thermo Fisher Scientific.

Ran cDNA constructs tagged to HA, including WT, T24N, and G19V forms in pKH3, were generously provided by Dr. Ian Macara (Vanderbilt University School of Medicine, Nashville, TN) (50). GSK3β cDNA constructs, including HA-tagged WT and S9A forms in pcDNA3, were generously provided by Dr. Jim Woodgett (Lunenfeld-Tanenbaum Research Institute/Mount Sinai Hospital, Toronto, Canada) (7). Rab7 constructs, including WT and T22N, were generously provided by Dr. Richard Pagano (Mayo Clinic and Foundation, Rochester, MN) (60).

Cell lines, cell culture, and inhibitor treatment

WT human retinal pigment epithelial cells (ARPE-19; herein referred to as RPE) were obtained from the American Type Culture Collection (ATCC, Manassas, VA) and cultured as described previously (77) with Dulbecco's modified Eagle's medium/F-12 (Gibco, Thermo Fisher Scientific) containing 10% fetal bovine serum, 100 units/ml penicillin and 100 μg/ml streptomycin. Cells were then incubated at 37 °C and 5% CO_2. MDA-MB-231 cells were obtained from ATCC and cultured as described previously (78) with RPMI medium 1640 (Gibco) containing 10% fetal bovine serum, 100 units/ml penicillin, and 100 μg/ml streptomycin and incubated at 37 °C and 5% CO_2.

All inhibitor treatments were performed (alone or in combination) for 1 h before experimental assays unless otherwise indicated, as follows: 10 μM CHIR99021 (Abcam, Cambridge, MA), 1 μM rapamycin (BioShop, Burlington, Canada), 10 μM LY294002 (Cell Signaling Technologies), 5 μM Akti-1/2 (Sigma-Aldrich, Oakville, Canada), 1 μM concanamycin A (BioShop). Amino acid starvation was performed by incubation in EBSS (Gibco).

Plasmid and siRNA transfections

To perform DNA plasmid transfections, Lipofectamine 2000 (Thermo Fisher Scientific) was used according to the manufacturer's instructions and as described previously (79). Briefly, cells were incubated for 4 h with Lipofectamine 2000 reagent and appropriate plasmid in Opti-MEM (Gibco) at a 3:1 ratio. Subsequently, this transfection solution was removed, and cells were incubated in fresh cell growth medium at 37 °C and 5% CO_2 for 16–24 h before experimentation.

To perform siRNA transfections as described previously (79), custom-synthesized siRNAs targeting specific transcripts with sequences as follows were obtained from Dharmacon (Lafayette, CO) as follows: nontargeting control, CGU ACU GCU UGC GAU ACG GUU (sense strand) and CGT ACT GCT TGC GAT ACG GUU (antisense strand); GSK3β, ACA CUA UAG UCG AGC CAA AUU (sense strand) and UUU GGC UCG ACU AUA GUG U (antisense strand); ULK1, GCA CAG AGA CCG UGG GCA AUU (sense strand) and UUG CCC ACG GUC UCU GUG CUU (antisense strand); APPL1, CAG AAU GUU CGC AGG GAA AUU (sense strand) and UUU CCC UGC GAA CAU UCU GUU (antisense strand). Cells were incubated with 220 pmol/liter of each siRNA sequence with Lipofectamine RNAiMAX (Life Technologies, Inc.) in Opti-MEM medium (Gibco) for 4 h at 37 °C and 5% CO_2. After this incubation period, cells were washed and incubated in fresh cell growth medium. siRNA transfections were performed twice, 72 and 48 h before experiments.

Whole-cell lysates, subcellular fractionation, and Western blotting

Western blotting using whole-cell lysates was performed as described previously (80). Cells were lysed in Laemmli sample buffer (0.5 M Tris, pH 6.8, glycerol, 5% bromphenol blue, 10% β-mercaptoethanol, 10% SDS; BioShop) containing phosphatase and protease mixture (1 mM sodium orthovanadate, 10 nM okadaic acid, and 20 nM protease inhibitor, all from BioShop). Cell lysates were then heated to 65 °C for 15 min and then passed through with a 27.5-gauge syringe. Proteins within whole-cell lysates were resolved by glycine-Tris SDS-PAGE and then transferred onto a polyvinylidene fluoride membrane, which was then incubated with a solution containing specific primary antibodies. Western blotting signal intensity detection corresponding to either phosphorylated proteins (*e.g.* pGSK3β Ser-9) or total proteins (*e.g.* GSK3β) and the respective loading controls (*e.g.* actin) was obtained by signal integration in an area corresponding to the specific lane and band for each condition. The measurement of phosphorylation of a specific protein was obtained by normalization of the signal intensity of a phosphorylated form of a protein to that of its loading control signal and then normalization to the signal intensity similarly obtained for the corresponding total protein.

To examine phosphorylation of proteins for which no specific antibodies were available, we used the phos-tag gel system, which results in exaggeration of differences in the apparent molecular weight of phosphorylated forms of specific proteins (56). The phos-tag reagent was obtained from Wako (Osaka, Japan) and was used in conjugation with SDS-PAGE polymerization as per the manufacturer's instructions. After SDS-PAGE was completed, gel was submerged in $MnCl_2$ for chelation of remaining phos-tag moieties. Subsequently, protein intensity detection, measurement, and processing were identical to steps mentioned above. Subcellular fractionation to isolate nuclear and cytoplasmic fractions was done using a nuclear extraction kit (catalog no. ab219177, Abcam), as per the manufacturer's instructions.

Immunofluorescence staining

Cells grown on glass coverslips were first subjected to fixation using cold methanol, blocked in 5% BSA (BioShop), and then stained with specific primary antibodies, followed by appropriate fluorophore-conjugated secondary antibody and counterstained with DAPI. Last, cells were then mounted on glass slides in fluorescence mounting medium (DAKO, Carpinteria, CA).

Fluorescence microscopy

Wide-field epifluorescence was performed on an Olympus IX83 inverted microscope with a ×100 objective, coupled to a Hamamatsu ORCA-Flash4.0 digital camera (Olympus Canada, Richmond Hill, Canada). Spinning disk confocal microscopy was performed using Quorum (Guelph, Canada) Diskovery combination total internal reflection fluorescence and spinning-disc confocal microscope, operating in spinning disc confocal mode. This instrument is composed of a Leica DMi8 microscope equipped with a ×63/1.49 numerical aperture objective with a ×1.8 camera relay (total magnification ×108). Imaging was done using 488-, 561-, and 637-nm laser illumination and 527/30, 630/75, and 700/75 emission filters and acquired using a Zyla 4.2Plus sCMOS camera (Hamamatsu).

SIM was performed using a Zeiss Elyra PS.1 superresolution inverted microscope, as described previously (81). Samples were imaged at an effective magnification of ×101 (×63 objective + ×1.6 Optovar tube lens) on an oil immersion objective. Typically, 25–35 slices of 0.110 μm were captured for each field of view for an imaging volume of ~2.75–3.85 μm. 488-, 561-, and 643-nm laser lines were directed into the microscope optical train via a multimode fiber coupler. The lasers were passed through a diffraction grating, and a series of diffraction orders (−1, 0, +1) were projected onto the back focal plane of the objective. These wave fronts were collimated in the objective to create a three-dimensional sinusoidal illumination pattern on the sample. The diffraction grating was then rotated and translated throughout the acquisition to create patterned offset images containing encoded high spatial frequency information. Five lateral positions were acquired at each of five (72°) diffraction grating rotations for a total of 25 raw images per *z*-plane. SIM imaging with all lasers was carried out at exposures varying

from 50 to 100 ms, with laser power varying between 3 and 10% (6–20 milliwatts at the output) and a gain level of 60–80. Imaging parameters were adjusted iteratively to achieve the best possible equalization of pixel intensity dynamic range across channels.

Raw SIM image stacks were processed in Zen under the Structured Illumination toolbar. A series of parameters were set to generate an optical transfer function used for three-dimensional reconstruction. The noise filter for Wiener deconvolution was set to a value of 1.0×10^{-4} to maximize the recovery of high spatial frequency information while minimizing illumination pattern artifacts. The maximum isotropy option was left unselected to recover all available frequency information at exactly the 72° rotation angles. Negative values arising as an artifact of the Wiener filter were clipped to zero using the Baseline Cut option. Processed SIM images were then aligned via an affine transformation matrix of predefined values obtained using 100-nm multicolor Tetraspeck fluorescent microspheres (Thermo Fisher Scientific).

Fluorescence microscopy image analysis

Total cellular signal intensity of specific proteins and GSK3β nuclear localization index were measured using ImageJ software (National Institutes of Health, Bethesda, MD). For total cellular measurements of specific protein signal, a region of interest corresponding to the cell outline, identified manually, was used to determine raw mean cellular fluorescence intensity. Final cellular signal intensity was obtained by subtracting background fluorescence (similarly obtained from a region on the coverslip with no cells) from the raw mean cellular fluorescence intensity, as described previously (52).

To determine GSK3β nuclear localization index, background-subtracted mean fluorescence intensity of regions of interest within the nucleus and cytoplasm were obtained. The GSK3β nuclear localization index is the ratio of these nuclear/cytosolic intensities. Each measurement was performed in at least three independent experiments, with >30 cells/condition/experiment. Colocalization analysis was performed by determination of Manders' or Pearson's coefficients, as indicated, using the Just Another Colocalization Plugin (82) within ImageJ, as described previously (79).

Quantification of GSK3β localization in LAMP1-positive membrane structures *versus* lysosome interior was performed (Fig. 6*D*) on two-color three-dimensional registered SIM images, which were split into single channel images consisting of GSK3β (red) or LAMP1 (green). To enhance the edge detection of LAMP1-associated membrane structures, a difference-of-Gaussians operation was performed on the LAMP1 images (83) ($\sigma_1 = 1$ pixel, $\sigma_2 = 3$ pixels). The resulting bandpass-filtered image was used to trace a selection around the membrane by identifying edges via pixel intensity line profiles in ImageJ. The resulting selection was then superimposed onto the original, unfiltered image, and a binary image mask was generated encompassing only the selected pixels identified as membrane-associated LAMP1. A binary image of the corresponding GSK3β channel was created by thresholding via the auto-threshold operation in ImageJ. The minimum cross entropy thresholding method (84) was selected, as it minimized the unnecessary removal of data (false negatives) and the inclusion of spurious intensity values (false positives). The area of each feature (GSK3β puncta) in the image was measured and recorded. Subsequently, an image subtraction operation was performed by subtracting pixels corresponding to LAMP1-positive membrane structures from the corresponding GSK3β channel. The area of the resulting GSK3β features was measured once again after the subtraction. Features for which a decrease in area was calculated were found to have pixels co-localizing with membrane-positive LAMP1 and thus were assigned as membrane-associated GSK3β. Features for which the area remained constant were deemed to be associated with either the cytosol (outside the LAMP1 membrane selection) or the lysosomal interior (inside the LAMP1 membrane selection).

Statistical analysis

Statistical analysis was performed as described previously (79). Measurement of samples involving two experimental conditions (Figs. 4*B* and 6 and Figs. S2, S3*A*, and S4*B*) were analyzed by Student's *t* test, with $p < 0.05$ as a threshold for statistically significant difference between conditions. Measurements of samples involving one experimental parameter and more than two conditions (Figs. 1, 2 (*B–D*), 4 (*A* and *C*), and 5*A* and Fig. S1 (*D* and *E*)) were analyzed by one-way analysis of variance, followed by Bonferonni post-test to compare differences between conditions, with $p < 0.05$ as a threshold for statistically significant difference between conditions. Measurements of samples involving two experimental parameters (Figs. 3, 4*D*, 5*B*, and 7 and Figs. S3*B* and S4*D*) were analyzed by two-way analysis of variance, followed by Bonferonni post-test to compare differences between conditions, with $p < 0.05$ as a threshold for statistically significant difference between conditions.

Author contributions—S. J. B. and C. N. A. conceptualization; S. J. B., I. B., A. V., and C. N. A. formal analysis; S. J. B., I. B., A. V., N. M., C. M. Y., P. K. K., and C. N. A. investigation; S. J. B., I. B., A. V., N. M., and C. N. A. methodology; S. J. B. and C. N. A. writing-original draft; S. J. B. and C. N. A. writing-review and editing; A. V. visualization; C. M. Y., P. K. K., and C. N. A. supervision; C. N. A. resources; C. N. A. data curation; C. N. A. funding acquisition; C. N. A. project administration.

Acknowledgments—We thank Dr. Jim Woodgett (Lunenfeld-Tanenbaum Research Institute/Mount Sinai Hospital, Toronto, Canada) and Dr. Sean Egan (Hospital for Sick Children, Toronto, Canada) for insightful and helpful discussions.

References

1. Beurel, E., Grieco, S. F., and Jope, R. S. (2015) Glycogen synthase kinase-3 (GSK3): regulation, actions, and diseases. *Pharmacol. Ther.* **148,** 114–131 CrossRef Medline
2. Doble, B. W., and Woodgett, J. R. (2003) GSK-3: tricks of the trade for a multi-tasking kinase. *J. Cell Sci.* **116,** 1175–1186 CrossRef Medline
3. Cormier, K. W., and Woodgett, J. R. (2017) Recent advances in understanding the cellular roles of GSK-3. *F1000Research* **6,** 167 CrossRef Medline
4. Sutherland, C. (2011) What are the *bona fide* GSK3 substrates? *Int. J. Alzheimers Dis.* **2011,** 1–23 CrossRef Medline

5. Jope, R. S., and Johnson, G. V. (2004) The glamour and gloom of glycogen synthase kinase-3. *Trends Biochem. Sci.* **29,** 95–102 CrossRef Medline
6. Linding, R., Jensen, L. J., Ostheimer, G. J., van Vugt, M. A. T. M., Jørgensen, C., Miron, I. M., Diella, F., Colwill, K., Taylor, L., Elder, K., Metalnikov, P., Nguyen, V., Pasculescu, A., Jin, J., Park, J. G., *et al.* (2007) Systematic discovery of *in vivo* phosphorylation networks. *Cell* **129,** 1415–1426 CrossRef Medline
7. Stambolic, V., and Woodgett, J. R. (1994) Mitogen inactivation of glycogen synthase kinase-3 β in intact cells via serine 9 phosphorylation. *Biochem. J.* **303**, 701–704 Medline
8. Cross, D. A., Alessi, D. R., Cohen, P., Andjelkovich, M., and Hemmings, B. A. (1995) Inhibition of glycogen synthase kinase-3 by insulin mediated by protein kinase B. *Nature* **378,** 785–789 CrossRef Medline
9. Tsujio, I., Tanaka, T., Kudo, T., Nishikawa, T., Shinozaki, K., Grundke-Iqbal, I., Iqbal, K., and Takeda, M. (2000) Inactivation of glycogen synthase kinase-3 by protein kinase C δ: implications for regulation of τ phosphorylation. *FEBS Lett.* **469,** 111–117 CrossRef Medline
10. Fang, X., Yu, S. X., Lu, Y., Bast, R. C., Jr., Woodgett, J. R., and Mills, G. B. (2000) Phosphorylation and inactivation of glycogen synthase kinase 3 by protein kinase A. *Proc. Natl. Acad. Sci. U.S.A.* **97,** 11960–11965 CrossRef Medline
11. Delcommenne, M., Tan, C., Gray, V., Rue, L., Woodgett, J., and Dedhar, S. (1998) Phosphoinositide-3-OH kinase–dependent regulation of glycogen synthase kinase 3 and protein kinase B/AKT by the integrin-linked kinase. *Proc. Natl. Acad. Sci. U.S.A.* **95,** 11211–11216 CrossRef Medline
12. Sutherland, C., Leighton, I. A., and Cohen, P. (1993) Inactivation of glycogen synthase kinase-3 β by phosphorylation: new kinase connections in insulin and growth-factor signalling. *Biochem. J.* **296**, 15–19
13. Thornton, T. M., Pedraza-Alva, G., Deng, B., Wood, C. D., Aronshtam, A., Clements, J. L., Sabio, G., Davis, R. J., Matthews, D. E., Doble, B., and Rincon, M. (2008) Phosphorylation by p38 MAPK as an alternative pathway for GSK3 inactivation. *Science* **320,** 667–670 CrossRef Medline
14. Meares, G. P., and Jope, R. S. (2007) Resolution of the nuclear localization mechanism of glycogen synthase kinase-3: functional effects in apoptosis. *J. Biol. Chem.* **282,** 16989–17001 CrossRef Medline
15. Bechard, M., and Dalton, S. (2009) Subcellular localization of glycogen synthase kinase 3β controls embryonic stem cell self-renewal. *Mol. Cell. Biol.* **29,** 2092–2104 CrossRef Medline
16. Gregory, M. A., Qi, Y., and Hann, S. R. (2003) Phosphorylation by glycogen synthase kinase-3 controls c-Myc proteolysis and subnuclear localization. *J. Biol. Chem.* **278,** 51606–51612 CrossRef Medline
17. Zhou, B. P., Deng, J., Xia, W., Xu, J., Li, Y. M., Gunduz, M., and Hung, M.-C. (2004) Dual regulation of Snail by GSK-3β-mediated phosphorylation in control of epithelial–mesenchymal transition. *Nat. Cell Biol.* **6,** 931–940 CrossRef Medline
18. Tang, Q.-Q., Grønborg, M., Huang, H., Kim, J.-W., Otto, T. C., Pandey, A., and Lane, M. D. (2005) Sequential phosphorylation of CCAAT enhancer-binding protein by MAPK and glycogen synthase kinase 3 is required for adipogenesis. *Proc. Natl. Acad. Sci. U.S.A.* **102,** 9766–9771 CrossRef Medline
19. Ross, S. E., Erickson, R. L., Hemati, N., and MacDougald, O. A. (1999) Glycogen synthase kinase 3 is an insulin-regulated C/EBPα kinase. *Mol. Cell. Biol.* **19,** 8433–8441 CrossRef Medline
20. Fiol, C. J., Williams, J. S., Chou, C. H., Wang, Q. M., Roach, P. J., and Andrisani, O. M. (1994) A secondary phosphorylation of CREB341 at Ser129 is required for the cAMP-mediated control of gene expression: a role for glycogen synthase kinase-3 in the control of gene expression. *J. Biol. Chem.* **269,** 32187–32193 Medline
21. Dang, C. V. (2012) MYC on the path to cancer. *Cell* **149,** 22–35 CrossRef Medline
22. Dang, C. V., Le, A., and Gao, P. (2009) MYC-induced cancer cell energy metabolism and therapeutic opportunities. *Clin. Cancer Res.* **15,** 6479–6483 CrossRef Medline
23. Kalkat, M., De Melo, J., Hickman, K. A., Lourenco, C., Redel, C., Resetca, D., Tamachi, A., Tu, W. B., and Penn, L. Z. (2017) MYC deregulation in primary human cancers. *Genes* (*Basel*) **8,** E151 CrossRef Medline
24. Thomas, L. R., and Tansey, W. P. (2011) Proteolytic control of the oncoprotein transcription factor Myc. *Adv. Cancer Res.* **110,** 77–106 CrossRef Medline
25. Zeng, X., Huang, H., Tamai, K., Zhang, X., Harada, Y., Yokota, C., Almeida, K., Wang, J., Doble, B., Woodgett, J., Wynshaw-Boris, A., Hsieh, J.-C., and He, X. (2008) Initiation of Wnt signaling: control of Wnt coreceptor Lrp6 phosphorylation/activation via frizzled, dishevelled and axin functions. *Development* **135,** 367–375 Medline
26. Wu, D., and Pan, W. (2010) GSK3: a multifaceted kinase in Wnt signaling. *Trends Biochem. Sci.* **35,** 161–168 CrossRef Medline
27. Schenck, A., Goto-Silva, L., Collinet, C., Rhinn, M., Giner, A., Habermann, B., Brand, M., and Zerial, M. (2008) The endosomal protein Appl1 mediates Akt substrate specificity and cell survival in vertebrate development. *Cell* **133,** 486–497 CrossRef Medline
28. Reis, C. R., Chen, P.-H., Srinivasan, S., Aguet, F., Mettlen, M., and Schmid, S. L. (2015) Crosstalk between Akt/GSK3β signaling and dynamin-1 regulates clathrin-mediated endocytosis. *EMBO J.* **34,** 2132–2146 CrossRef Medline
29. Li, Y., Xu, M., Ding, X., Yan, C., Song, Z., Chen, L., Huang, X., Wang, X., Jian, Y., Tang, G., Tang, C., Di, Y., Mu, S., Liu, X., Liu, K., *et al.* (2016) Protein kinase C controls lysosome biogenesis independently of mTORC1. *Nat. Cell Biol.* **18,** 1065–1077 CrossRef Medline
30. Azoulay-Alfaguter, I., Elya, R., Avrahami, L., Katz, A., and Eldar-Finkelman, H. (2015) Combined regulation of mTORC1 and lysosomal acidification by GSK-3 suppresses autophagy and contributes to cancer cell growth. *Oncogene* **34,** 4613–4623 CrossRef Medline
31. Bijur, G. N., and Jope, R. S. (2001) Proapoptotic stimuli induce nuclear accumulation of glycogen synthase kinase-3β. *J. Biol. Chem.* **276,** 37436–37442 CrossRef Medline
32. Diehl, J. A., Cheng, M., Roussel, M. F., and Sherr, C. J. (1998) Glycogen synthase kinase-3β regulates cyclin D1 proteolysis and subcellular localization. *Genes Dev.* **12,** 3499–3511 CrossRef Medline
33. Zmijewski, J. W., and Jope, R. S. (2004) Nuclear accumulation of glycogen synthase kinase-3 during replicative senescence of human fibroblasts. *Aging Cell* **3,** 309–317 CrossRef Medline
34. Inoki, K., Li, Y., Zhu, T., Wu, J., and Guan, K.-L. (2002) TSC2 is phosphorylated and inhibited by Akt and suppresses mTOR signalling. *Nat. Cell Biol.* **4,** 648–657 CrossRef Medline
35. Inoki, K., Li, Y., Xu, T., and Guan, K.-L. (2003) Rheb GTPase is a direct target of TSC2 GAP activity and regulates mTOR signaling. *Genes Dev.* **17,** 1829–1834 CrossRef Medline
36. Long, X., Lin, Y., Ortiz-Vega, S., Yonezawa, K., and Avruch, J. (2005) Rheb binds and regulates the mTOR kinase. *Curr. Biol.* **15,** 702–713 CrossRef Medline
37. Tee, A. R., Manning, B. D., Roux, P. P., Cantley, L. C., and Blenis, J. (2003) Tuberous sclerosis complex gene products, Tuberin and Hamartin, control mTOR signaling by acting as a GTPase-activating protein complex toward Rheb. *Curr. Biol.* **13,** 1259–1268 CrossRef Medline
38. Saxton, R. A., and Sabatini, D. M. (2017) mTOR signaling in growth, metabolism, and disease. *Cell* **168,** 960–976 CrossRef Medline
39. Zoncu, R., Bar-Peled, L., Efeyan, A., Wang, S., Sancak, Y., and Sabatini, D. M. (2011) mTORC1 senses lysosomal amino acids through an inside-out mechanism that requires the vacuolar H^+-ATPase. *Science* **334,** 678–683 CrossRef Medline
40. Bar-Peled, L., Schweitzer, L. D., Zoncu, R., and Sabatini, D. M. (2012) Ragulator is a GEF for the Rag GTPases that signal amino acid levels to mTORC1. *Cell* **150,** 1196–1208 CrossRef Medline
41. Shaw, R. J., Bardeesy, N., Manning, B. D., Lopez, L., Kosmatka, M., DePinho, R. A., and Cantley, L. C. (2004) The LKB1 tumor suppressor negatively regulates mTOR signaling. *Cancer Cell* **6,** 91–99 CrossRef Medline
42. Inoki, K., Ouyang, H., Zhu, T., Lindvall, C., Wang, Y., Zhang, X., Yang, Q., Bennett, C., Harada, Y., Stankunas, K., Wang, C. Y., He, X., MacDougald, O. A., You, M., Williams, B. O., and Guan, K.-L. (2006) TSC2 integrates Wnt and Energy signals via a coordinated phosphorylation by AMPK and GSK3 to regulate cell growth. *Cell* **126,** 955–968 CrossRef Medline
43. Stretton, C., Hoffmann, T. M., Munson, M. J., Prescott, A., Taylor, P. M., Ganley, I. G., and Hundal, H. S. (2015) GSK3-mediated raptor phosphor-

ylation supports amino-acid-dependent mTORC1-directed signalling. *Biochem. J.* **470,** 207–221 CrossRef Medline
44. Ka, M., Condorelli, G., Woodgett, J. R., and Kim, W.-Y. (2014) mTOR regulates brain morphogenesis by mediating GSK3 signaling. *Development* **141,** 4076–4086 CrossRef Medline
45. Suzuki, T., Bridges, D., Nakada, D., Skiniotis, G., Morrison, S. J., Lin, J. D., Saltiel, A. R., and Inoki, K. (2013) Inhibition of AMPK catabolic action by GSK3. *Mol. Cell.* **50,** 407–419 CrossRef Medline
46. Smith, K. P., Byron, M., O'Connell, B. C., Tam, R., Schorl, C., Guney, I., Hall, L. L., Agrawal, P., Sedivy, J. M., and Lawrence, J. B. (2004) c-Myc localization within the nucleus: evidence for association with the PML nuclear body. *J. Cell. Biochem.* **93,** 1282–1296 CrossRef Medline
47. Abrams, H. D., Rohrschneider, L. R., and Eisenman, R. N. (1982) Nuclear location of the putative transforming protein of avian myelocytomatosis virus. *Cell* **29,** 427–439 CrossRef Medline
48. Hann, S. R., Abrams, H. D., Rohrschneider, L. R., and Eisenman, R. N. (1983) Proteins encoded by v-myc and c-myc oncogenes: identification and localization in acute leukemia virus transformants and bursal lymphoma cell lines. *Cell* **34,** 789–798 CrossRef Medline
49. Woodgett, J. R. (1990) Molecular cloning and expression of glycogen synthase kinase-3/factor A. *EMBO J.* **9,** 2431–2438 Medline
50. Carey, K. L., Richards, S. A., Lounsbury, K. M., and Macara, I. G. (1996) Evidence using a green fluorescent protein-glucocorticoid receptor chimera that the Ran/TC4 GTPase mediates an essential function independent of nuclear protein import. *J. Cell Biol.* **133,** 985–996 CrossRef Medline
51. Inoki, K., Kim, J., and Guan, K.-L. (2012) AMPK and mTOR in cellular energy homeostasis and drug targets. *Annu. Rev. Pharmacol. Toxicol.* **52,** 381–400 CrossRef Medline
52. Ross, E., Ata, R., Thavarajah, T., Medvedev, S., Bowden, P., Marshall, J. G., and Antonescu, C. N. (2015) AMP-activated protein kinase regulates the cell surface proteome and integrin membrane traffic. *PLoS One* **10,** e0128013 CrossRef Medline
53. Jung, C. H., Jun, C. B., Ro, S.-H., Kim, Y.-M., Otto, N. M., Cao, J., Kundu, M., and Kim, D.-H. (2009) ULK-Atg13-FIP200 complexes mediate mTOR signaling to the autophagy machinery. *Mol. Biol. Cell.* **20,** 1992–2003 CrossRef Medline
54. Saric, A., Hipolito, V. E. B., Kay, J. G., Canton, J., Antonescu, C. N., and Botelho, R. J. (2016) MTOR controls lysosome tubulation and antigen presentation in macrophages and dendritic cells. *Mol. Biol. Cell.* **27,** 321–333 CrossRef Medline
55. Cianfanelli, V., Fuoco, C., Lorente, M., Salazar, M., Quondamatteo, F., Gherardini, P. F., De Zio, D., Nazio, F., Antonioli, M., D'Orazio, M., Skobo, T., Bordi, M., Rohde, M., Dalla Valle, L., Helmer-Citterich, M., *et al.* (2015) AMBRA1 links autophagy to cell proliferation and tumorigenesis by promoting c-Myc dephosphorylation and degradation. *Nat. Cell Biol.* **17,** 20–30 CrossRef Medline
56. Kinoshita, E., Kinoshita-Kikuta, E., Takiyama, K., and Koike, T. (2006) Phosphate-binding tag, a new tool to visualize phosphorylated proteins. *Mol. Cell. Proteomics* **5,** 749–757 CrossRef Medline
57. Sancak, Y., Peterson, T. R., Shaul, Y. D., Lindquist, R. A., Thoreen, C. C., Bar-Peled, L., and Sabatini, D. M. (2008) The Rag GTPases bind Raptor and mediate amino acid signaling to mTORC1. *Science* **320,** 1496–1501 CrossRef Medline
58. Kaushik, S., Massey, A. C., and Cuervo, A. M. (2006) Lysosome membrane lipid microdomains: novel regulators of chaperone-mediated autophagy. *EMBO J.* **25,** 3921–3933 CrossRef Medline
59. Chu, B.-B., Liao, Y.-C., Qi, W., Xie, C., Du, X., Wang, J., Yang, H., Miao, H.-H., Li, B.-L., and Song, B.-L. (2015) Cholesterol transport through lysosome-peroxisome membrane contacts. *Cell* **161,** 291–306 CrossRef Medline
60. Choudhury, A., Dominguez, M., Puri, V., Sharma, D. K., Narita, K., Wheatley, C. L., Marks, D. L., and Pagano, R. E. (2002) Rab proteins mediate Golgi transport of caveola-internalized glycosphingolipids and correct lipid trafficking in Niemann-Pick C cells. *J. Clin. Invest.* **109,** 1541–1550 CrossRef Medline
61. Zoncu, R., Perera, R. M., Balkin, D. M., Pirruccello, M., Toomre, D., and De Camilli, P. (2009) A phosphoinositide switch controls the maturation and signaling properties of APPL endosomes. *Cell* **136,** 1110–1121 CrossRef Medline
62. Taelman, V. F., Dobrowolski, R., Plouhinec, J.-L., Fuentealba, L. C., Vorwald, P. P., Gumper, I., Sabatini, D. D., and De Robertis, E. M. (2010) Wnt signaling requires sequestration of glycogen synthase kinase 3 inside multivesicular endosomes. *Cell* **143,** 1136–1148 CrossRef Medline
63. Vanlandingham, P. A., and Ceresa, B. P. (2009) Rab7 regulates late endocytic trafficking downstream of multivesicular body biogenesis and cargo sequestration. *J. Biol. Chem.* **284,** 12110–12124 CrossRef Medline
64. Azoulay-Alfaguter, I., Yaffe, Y., Licht-Murava, A., Urbanska, M., Jaworski, J., Pietrokovski, S., Hirschberg, K., and Eldar-Finkelman, H. (2011) Distinct molecular regulation of glycogen synthase kinase-3α isozyme controlled by its N-terminal region: functional role in calcium/calpain signaling. *J. Biol. Chem.* **286,** 13470–13480 CrossRef Medline
65. Franca-Koh, J., Yeo, M., Fraser, E., Young, N., and Dale, T. C. (2002) The regulation of glycogen synthase kinase-3 nuclear export by Frat/GBP. *J. Biol. Chem.* **277,** 43844–43848 CrossRef Medline
66. Strambio-De-Castillia, C., Niepel, M., and Rout, M. P. (2010) The nuclear pore complex: bridging nuclear transport and gene regulation. *Nat. Rev. Mol. Cell Biol.* **11,** 490–501 CrossRef Medline
67. Ding, Q., Xia, W., Liu, J.-C., Yang, J.-Y., Lee, D.-F., Xia, J., Bartholomeusz, G., Li, Y., Pan, Y., Li, Z., Bargou, R. C., Qin, J., Lai, C.-C., Tsai, F.-J., Tsai, C.-H., and Hung, M.-C. (2005) Erk associates with and primes GSK-3β for its inactivation resulting in upregulation of β-catenin. *Mol. Cell* **19,** 159–170 CrossRef Medline
68. Stadler, S. C., Vincent, C. T., Fedorov, V. D., Patsialou, A., Cherrington, B. D., Wakshlag, J. J., Mohanan, S., Zee, B. M., Zhang, X., Garcia, B. A., Condeelis, J. S., Brown, A. M. C., Coonrod, S. A., and Allis, C. D. (2013) Dysregulation of PAD4-mediated citrullination of nuclear GSK3β activates TGF-β signaling and induces epithelial-to-mesenchymal transition in breast cancer cells. *Proc. Natl. Acad. Sci. U.S.A.* **110,** 11851–11856 CrossRef Medline
69. Feijs, K. L., Kleine, H., Braczynski, A., Forst, A. H., Herzog, N., Verheugd, P., Linzen, U., Kremmer, E., and Lüscher, B. (2013) ARTD10 substrate identification on protein microarrays: regulation of GSK3β by mono-ADP-ribosylation. *Cell Commun. Signal.* **11,** 5 CrossRef Medline
70. Goñi-Oliver, P., Lucas, J. J., Avila, J., and Hernández, F. (2007) N-terminal cleavage of GSK-3 by calpain: a new form of GSK-3 regulation. *J. Biol. Chem.* **282,** 22406–22413 CrossRef Medline
71. Flinn, R. J., Yan, Y., Goswami, S., Parker, P. J., and Backer, J. M. (2010) The late endosome is essential for mTORC1 signaling. *Mol. Biol. Cell.* **21,** 833–841 CrossRef Medline
72. Lüscher, B., and Eisenman, R. N. (1988) c-myc and c-myb protein degradation: effect of metabolic inhibitors and heat shock. *Mol. Cell. Biol.* **8,** 2504–2512 CrossRef Medline
73. Miller, D. M., Thomas, S. D., Islam, A., Muench, D., and Sedoris, K. (2012) c-Myc and cancer metabolism. *Clin. Cancer Res.* **18,** 5546–5553 CrossRef Medline
74. Cho, K. B., Cho, M. K., Lee, W. Y., and Kang, K. W. (2010) Overexpression of c-myc induces epithelial mesenchymal transition in mammary epithelial cells. *Cancer Lett.* **293,** 230–239 CrossRef Medline
75. Sekiya, S., and Suzuki, A. (2011) Glycogen synthase kinase 3 β-dependent Snail degradation directs hepatocyte proliferation in normal liver regeneration. *Proc. Natl. Acad. Sci. U.S.A.* **108,** 11175–11180 CrossRef Medline
76. Nikolakaki, E., Coffer, P. J., Hemelsoet, R., Woodgett, J. R., and Defize, L. H. (1993) Glycogen synthase kinase 3 phosphorylates Jun family members *in vitro* and negatively regulates their transactivating potential in intact cells. *Oncogene* **8,** 833–840 Medline
77. Delos Santos, R. C., Bautista, S., Lucarelli, S., Bone, L. N., Dayam, R. M., Botelho, R. J., and Antonescu, C. N. (2017) Selective control of clathrin-mediated endocytosis and clathrin-dependent signaling by phospholipase C and Ca^{2+} signals. *Mol. Biol. Cell.* **28,** 2802–2818 CrossRef Medline
78. Fekri, F., Delos Santos, R. C., Karshafian, R., and Antonescu, C. N. (2016) Ultrasound microbubble treatment enhances clathrin-mediated endocytosis and fluid-phase uptake through distinct mechanisms. *PLoS One* **11,** e0156754 CrossRef Medline

79. Bone, L. N., Dayam, R. M., Lee, M., Kono, N., Fairn, G. D., Arai, H., Botelho, R. J., and Antonescu, C. N. (2017) The acyltransferase LYCAT controls specific phosphoinositides and related membrane traffic. *Mol. Biol. Cell.* **28,** 161–172 CrossRef Medline
80. Garay, C., Judge, G., Lucarelli, S., Bautista, S., Pandey, R., Singh, T., and Antonescu, C. N. (2015) Epidermal growth factor-stimulated Akt phosphorylation requires clathrin or ErbB2 but not receptor endocytosis. *Mol. Biol. Cell.* **26,** 3504–3519 CrossRef Medline
81. Hua, R., Cheng, D., Coyaud, É., Freeman, S, Di Pietro, E., Wang, Y., Vissa, A., Yip, C. M., Fairn, G. D., Braverman, N., Brumell, J. H., Trimble, W. S., Raught, B., and Kim, P. K. (2017) VAPs and ACBD5 tether peroxisomes to the ER for peroxisome maintenance and lipid homeostasis. *J. Cell Biol.* **216,** 367–377 CrossRef Medline
82. Bolte, S., and Cordelières, F. P. (2006) A guided tour into subcellular colocalization analysis in light microscopy. *J. Microsc.* **224,** 213–232 CrossRef Medline
83. Marr, D., and Hildreth, E. (1980) Theory of edge detection. *Proc. R. Soc. London. Ser. B Biol. Sci.* **207,** 187–217 CrossRef Medline
84. Li, C. H., and Tam, P. K. S. (1998) An iterative algorithm for minimum cross entropy thresholding. *Pattern Recognit. Lett.* **19,** 771–776 CrossRef